CALCULATION OF ION ENERGY-DEPOSITION SPECTRA IN SILICON, LITHIUM-FLUORIDE, BORON, AND BORON CARBIDE

by

J.K. Shultis and D.S. McGregor

Department of Mechanical and Nuclear Engineering
Kansas State University
Manhattan, Kansas 55606

published as

Report 299

ENGINEERING EXPERIMENT STATION

College of Engineering
Kansas State University
Manhattan, Kansas 66506

April 2004
Corrected January and July 2007

ABSTRACT

The ions produced by the thermal neutron reactions $^{10}\mathrm{B}(n,\alpha)^{7}\mathrm{Li}$ and $^{6}\mathrm{Li}(n,t)^{4}\mathrm{He}$ are used to detect neutrons and to infer concentration profiles of boron and lithium beneath a surface. In both applications it is important to be able to calculate the energy deposited in the medium through which the ions pass.

In this report empirical formulas are presented that allow rapid calculation of (1) the stopping power for the ions, (2) their residual energy after traveling a specified distance, (3) the path length needed to reduce their initial energy to any lower energy, and (4) the energy straggling as a function of their energy. Results are presented for media of boron, lithium fluoride, and silicon.

A Monte Carlo procedure for calculating the energy-deposition spectrum in various materials is presented and then applied to the design of silicon-based semiconductor detectors. Several novel geometries for incorporating the neutron reactive material (boron or lithium fluoride) intimately with the semiconductor material are considered. Specifically, the energy deposited in the semiconductor by the ions born in the converter material are calculated and the overall thermal-neutron detection efficiency estimated. Several example energy-deposition spectra are presented.

From these results it appears that small semiconductor detectors can be constructed with thermal-neutron detection efficiencies of well over 50%, a value many times greater than presently available with these type of devices.

Contents

Calculation of Ion Energy-Deposition Spectra in Silicon, Lithium-Fluoride, and Boron

J. Kenneth Shultis and Douglas McGregor

April 2004

Introduction

The calculation of the energy deposited by ions produced by thermal neutron interactions in various materials is needed in several applications. For example, in neutron depth profiling the energy of reaction product ions escaping a sample's surface provides information about the concentration profile, as a function of depth into the surface, of the isotope that interacts with the incident neutrons [Shultis 2003, 2004]. In the design of solid-state thermal-neutron detectors, the energy deposited by reaction product ions in the detector material is of importance to both identify the proper operation of the detector and to estimate the detector efficiencies for different device designs [McGregor et al. 2003; McGregor and Shultis 2004].

In this report, methods are summarized for estimating how much energy is deposited by ions born in one region (or material) and that subsequently enter a second region or material. In particular, ions born through (n,α) reactions in a converter region containing ^{10}B or ions born from (n,t) reactions in regions containing ^{6}Li are considered. For neutron depth profiling studies and for bulk solid-state detectors (in which the converter material is also the detector material), the energy lost in the converter material is also of interest. By contrast, for coated semiconductor detectors, the ions are produced in a converter material adjacent to the semiconductor material so that the energy deposited in the semiconductor is of interest.

In this report methods for calculating the energy deposited in various detector regions are presented. From these calculations, the thermal neutron detection efficiency can be estimated for different detector designs. From these efficiency calculations, novel detector designs are then proposed that have a vast increase in efficiency compared to that for presently available semiconductor devices.

1 The Ion Producing Reactions

There are several light isotopes with which thermal neutrons interact to produce energetic ion reaction products. In this report we consider two particular (n,α) reactions that have large thermal neutron cross sections and, consequently, are ideally suited as a converter material in neutron detectors or for measurement in NDP studies.

1.1 The ^{10}B(n,α)^{7}Li Reaction

The isotope ^{10}B has a large thermal-neutron cross section (3840 b at 0.00253 eV) for the ^{10}B(n,α)^{7}Li reaction. Two distinct energies of α and ^{7}Li ions are produced since the ^{7}Li nucleus is produced either in the ground state or in a 0.4776-MeV excited state as shown below.

$$ {}^1_0\mathrm{n} + {}^{10}_5\mathrm{B} \longrightarrow \begin{cases} {}^7_3\mathrm{Li}^* \,(1.4721\text{ MeV}) + {}^4_2\mathrm{He}\,(0.8398\text{ MeV}) & Q = 2.3119\text{ MeV } (93.7\%) \\ {}^7_3\mathrm{Li}\,(1.7762\text{ MeV}) + {}^4_2\mathrm{He}\,(1.0133\text{ MeV}) & Q = 2.7895\text{ MeV } (6.3\%) \end{cases} $$

Alpha particles are produced with the two energies 1.7762 MeV (α_1) and 1.4721 MeV (α_2). The corresponding lithium ions have energies 1.0133 MeV (Li_1) and 0.8398 MeV (Li_2).

1.2 The ^{6}Li(n, t)^{4}He Reaction

The isotope ^{6}Li also has a large thermal-neutron cross section (940 b at 0.00253 eV) for the ^{6}Li(n,α)^{7}H reaction shown below.

$$^1_0\mathrm{n} + ^6_3\mathrm{Li} \longrightarrow ^3_1\mathrm{H}\,(2.7276\ \mathrm{MeV}) + ^4_2\mathrm{He}\,(2.0553\ \mathrm{MeV}) \qquad Q = 4.7829\ \mathrm{MeV}$$

1.3 Ranges of Reaction Ions

In Table 1 the thermal neutron attenuation properties of the three converter materials considered in this study are summarized. Then in Table 2, the ranges of the various reaction ions in the different materials are tabulated. These ranges were calculated by the TRIM code [Ziegler and Biersack 2002] for the material densities shown in Table 1 and represent the maximum distance a reaction-product ion travels in the material. The TRIM ranges, consequently, are slightly larger than the usual extrapolated and mean ion ranges.

Table 1. Density and the 2200 m/s and thermal-averaged (n, α) cross sections of three converter materials. $\overline{\Sigma}_{(n,\alpha)}$ is for a room temperature (293 K) Maxwellian distribution of thermal neutrons.

Material	ρ (g/cm^3	$\sigma_{(n,\alpha)}(E_o)$ (b)	$\Sigma_{(n,\alpha)}(E_o)$ (cm^{-1})	$\overline{\Sigma}_{(n,\alpha)}$ (cm^{-1})
^{6}LiF	2.54	940	57.3	50.0
^{10}B	2.14	3840	494	438
^{10}B$_4$C	2.52	3840	84.0	74.4

Table 2. Ion ranges as calculated by the TRIM code. The material densities for the converter materials are those listed in Table 1 and that for silicon is $\rho = 2.32$ g/cm^3.

Ion	Reaction	Initial energy (MeV)	Range (μm)			
			^{10}B	^{10}B$_4$C	^{6}LiF	Si
α_1	^{10}B$(n,\alpha)^7$Li	1.7762	4.80	4.12	5.41	6.34
α_2	^{10}B$(n,\alpha)^7$Li	1.4721	3.89	3.34	4.52	5.16
Li_1	^{10}B$(n,\alpha)^7$Li	1.0133	2.26	1.90	2.85	2.81
Li_2	^{10}B$(n,\alpha)^7$Li	0.8398	2.01	1.69	2.55	2.46
α	^{6}Li$(n,t)^4$He	2.0553	5.70	4.88	6.29	7.51
Li	^{6}Li$(n,t)^4$He	2.7276	35.8	30.1	34.7	42.9

2 Empirical Fits for Selected Ion Data

The analysis of ion energy-deposition spectra obtained using the neutron depth profiling (NDP) technique to obtain ^{10}B concentration profiles in silicon samples requires knowledge of how the alpha ^{4}He and ^{7}Li ions produced in the ^{10}B$(n,\alpha)^7$Li reaction interact in silicon. Also for estimating ion energy-deposition spectra in semiconductor detectors it is necessary to be able to rapidly calculate

certain various interaction properties of the reaction ions in various materials. Specifically, one needs (1) the stopping power $S(E)$ of the ions at all energies, (2) the residual energy $\overline{E}(x)$ of an ion after travelling a distance x less than its range, (3) the path length $\overline{X}(E)$ required to reduce an ion from its initial energy any lower energy E, and (4) the energy straggling (measured by the standard deviation of the ion energy $\sigma_{str}(\overline{E}(x))$ after travelling a distance x in silicon.

The SRIM Monte Carlo code package [Ziegler and Biersack 2002] provides such ion-interaction data. With this package, interaction data for helium and lithium ions in silicon was obtained, and empirical formulas were fitted to these data. The fitting was performed using TableCurve [Jandel 1998] which fits many thousands of different equations to the given data and then ranks the fits according the degree of agreement between the fit and data (here a χ^2 statistic). The selected fit was chosen by selecting the fit with relatively few free parameters and that had good agreement with the data, The results of these empirical fits are reported in the following subsections.

2.1 Empirical Results for Silicon

2.1.1 Stopping Power in Silicon

An empirical formula for the stopping power in silicon is

$$S(E) \equiv \left(-\frac{dE}{ds}\right) = \frac{a + cE + eE^2}{1 + bE + dE^2 + fE^3}, \tag{1}$$

where $S(E)$ has units of keV/μm and E is the ion energy in MeV. Equation 1 is valid for $0.01 \leq E \leq 2$ MeV for ^{4}He and ^{7}Li ions. For ^{3}H ions the fit is valid up to 5 MeV. Parameters for this fitting formula are given in Table 3 and a comparison of the fit to the TRIM data is shown in Fig. 1.

Table 3. Parameters for the empirical formula of Eq. (1) for the stopping power in silicon for three ions.

Parameter in Eq. (1)	^{4}He ion	^{7}Li ion	^{3}H ion
a	31.061478	68.389815	28.123689
b	1.8137558	−0.037458064	7.05870508
c	1862.3846	974.00508	2036.16929
d	14.803816	3.9534614	52.2576323
e	4772.0507	1454.8708	3446.58601
f	3.735421	−0.21760158	15.7007858

2.1.2 Residual Energy in Silicon

An empirical formula that gives the residual energy (MeV) of the four ^{10}B$(n,\alpha)^7$Li ions after they have traveled a distance x (μm) in silicon is

$$\overline{E}(x) = \frac{a + cx + ex^2}{1 + bx + dx^2 + fx^3}. \tag{2}$$

This same equation is also a good approximation for the α particle produced in the ^{6}Li$(n,t)^4$He reaction. However, it is a poor approximation for the triton produced in this reaction. For the triton a good approximating formula is

$$\overline{E}(x) = \exp\left[\frac{a + cx + ex^2}{1 + bx + dx^2}\right]. \tag{3}$$

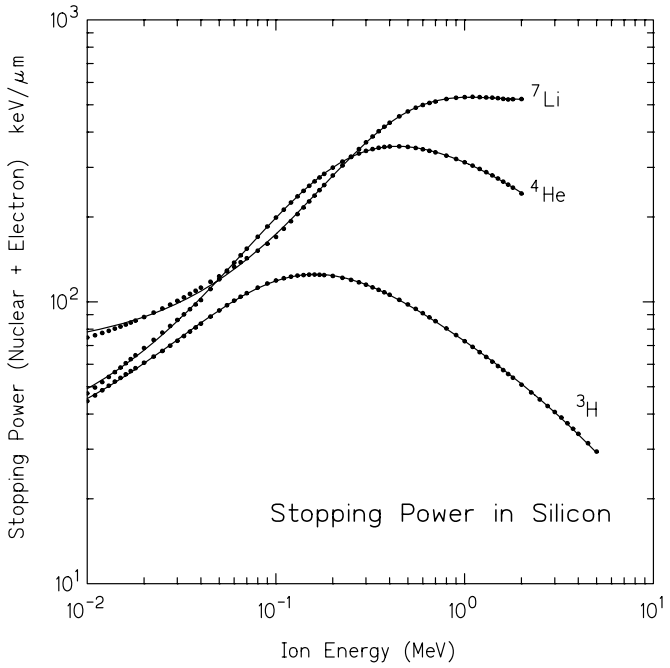

Figure 1. Stopping power $S(E) = -dE/ds$ for ^{3}H, ^{4}He and ^{7}Li ions in silicon. Circles are data calculated by the TRIM code and lines are the empirical fits of Eq. (1).

where again x is in units of μm.

Parameters for this fitting formula are given in Table 4 and a comparisons of the fits to the TRIM data are shown in Figs. 2 and 3.

Table 4. Values of the parameters for the empirical formulas of Eq. (2) and Eq. (3) for the residual ion energies in silicon.

Parm	^{10}B$(n,\alpha)^7$Li				^{6}Li$(n,t)^4$He	
	α_1 [Eq. (2)]	α_2 [Eq. (2)]	Li$_1$ [Eq. (2)]	Li$_2$ [Eq. (2)]	α [Eq. (2)]	^{3}H [Eq. (3)]
a	1.7785882	1.4731692	1.0132997	0.83979996	2.0549684169	0.99849937868
b	-0.16516657	-0.18960846	487.60039	7308.0497	-0.1483764308	-0.03278510295
c	-0.56309544	-0.56619005	476.75505	6150.5345	-0.5570727178	-0.04902551060
d	-0.0020145557	-0.0028652391	9.1891196	1456.6053	-0.0005753511	0.00022141343
e	0.044594767	0.054390703	-168.03407	-2421.0822	0.0377800136	0.00054282700
f	0.0015759151	0.0032178631	129.50593	1899.8145	0.0007588408	

2.1.3 Path Length in Silicon to Reach a Specified Residual Energy

An empirical formula that gives the path length x (μm) in silicon for ^{10}B$(n,\alpha)^7$Li ions to reach residual energy E (MeV) is

$$\overline{X}(E) = a + bE + cE^{1.5} + dE^3 + c\exp(-E). \tag{4}$$

Parameters for this fitting formula are given in Table 5 and a comparison of the fit to the TRIM data is shown in Fig. 4.

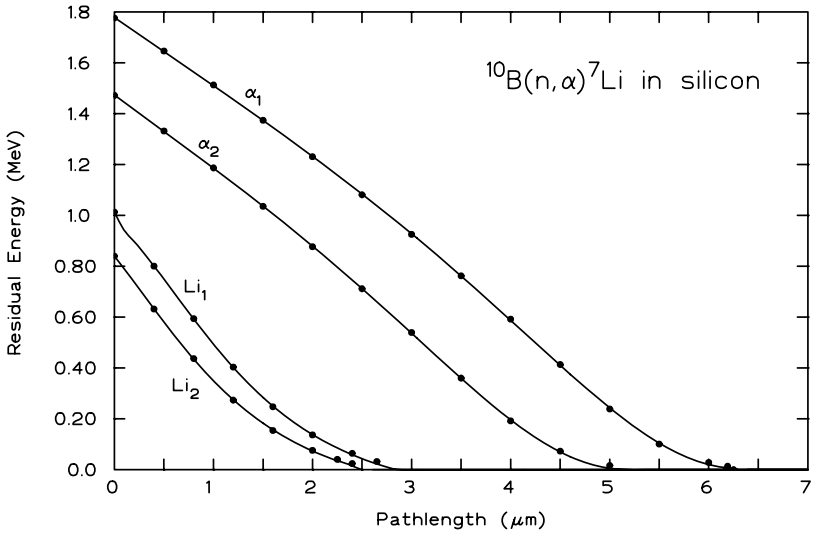

Figure 2. Residual energy of $^{10}\mathrm{B}(n,\alpha)^{6}\mathrm{Li}$ product ions after travelling through silicon. Circles are data calculated by the TRIM code and lines are the empirical fits of Eq. (2).

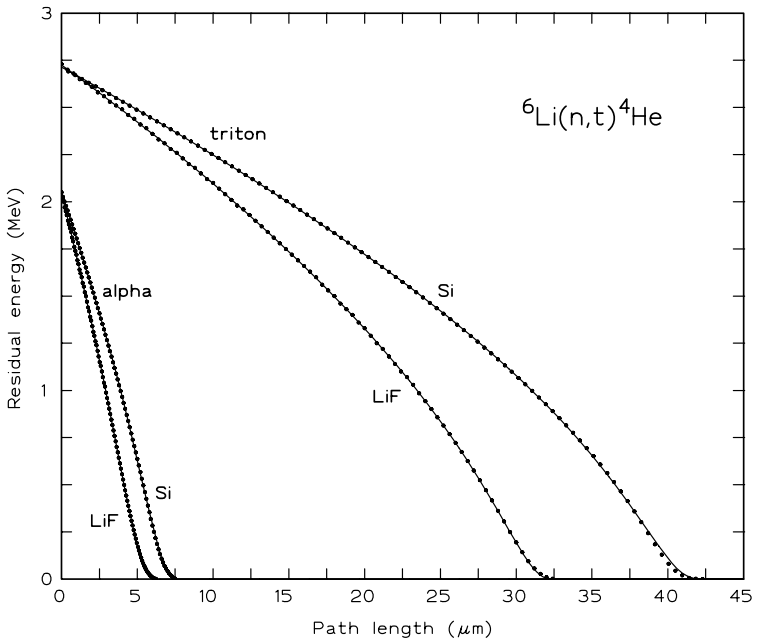

Figure 3. Residual energy of the $^{6}\mathrm{Li}(n,t)^{4}\mathrm{He}$ product ions after travelling through silicon and LiF. Circles are data calculated by the TRIM code and lines are the empirical fits of Eq. (2) for the α particle and of Eq. (3) for the triton.

For the $^6\mathrm{Li}(n,t)^4\mathrm{He}$ ions different empirical formulas must be used. For the α particle, $\overline{X}(E)$ is given by

$$\overline{X}(E) = a + b\sqrt{E} + cE + dE^{3/2} + eE^2 + fE^{5/2} + gE^3, \tag{5}$$

and, for the triton, by

$$\overline{X}(E) = a + bE + cE^2 + dE^2 \ln E + e\sqrt{E} \ln E. \tag{6}$$

In both of these approximations, E is in units of MeV. Values of the fitting parameters are given in Table 6 and the empirical approximations are compared to the TRIM data in Fig. 5.

Table 5. Parameters for the empirical formula of Eq. (4) for the path length needed to reach a given residual energy in silicon.

Parameter in Eq. (4)	α_1	α_2	Li_1	Li_2
a	52.018871	53.546724	16.994645	0.10642838
b	-59.738396	-62.762173	-24.033867	-6.1114722
c	28.198743	29.509255	13.40238	6.8549249
d	-0.87714178	-0.85902922	-1.1234069	-2.10642838
e	-45.762079	-48.443298	-14.176564	2.3973523

Table 6. Parameters for the empirical formula of Eq. (5) and Eq. (6) for the path length needed to reach a given residual energy in silicon.

Parameter	^{4}He ion: Eq. (5)	^{3}H ion: Eq. (6)
a	7.650654782456231	42.55432730826800
b	-2.951907906029242	6.126822912741065
c	-3.226254043595208	-5.405288206496186
d	12.90757367270686	1.274522449649497
e	-19.00554784825017	2.744516841023055
f	10.85346324881674	
g	-2.337319132539310	

2.1.4 Spectral Broadening from Energy Straggling in Silicon

The broadening of ion energies caused by energy straggling was investigated using the Monte Carlo TRIM code of the SRIM package [Ziegler and Biersack 2002]. For a specified thickness x of silicon, the exit energies of normally incident alpha and lithium ions were recorded. Based on $N \geq 10,000$ histories, the standard deviation of transmitted particle energies was computed as

$$\sigma_{str}^2 = \frac{1}{N-1} \sum_{i=1}^{N} (E_i - \overline{E})^2, \tag{7}$$

where E_i is the energy of the ith transmitted ion and the mean transmitted energy is $\overline{E} = \sum_{i=1}^{N} E_i/N$.

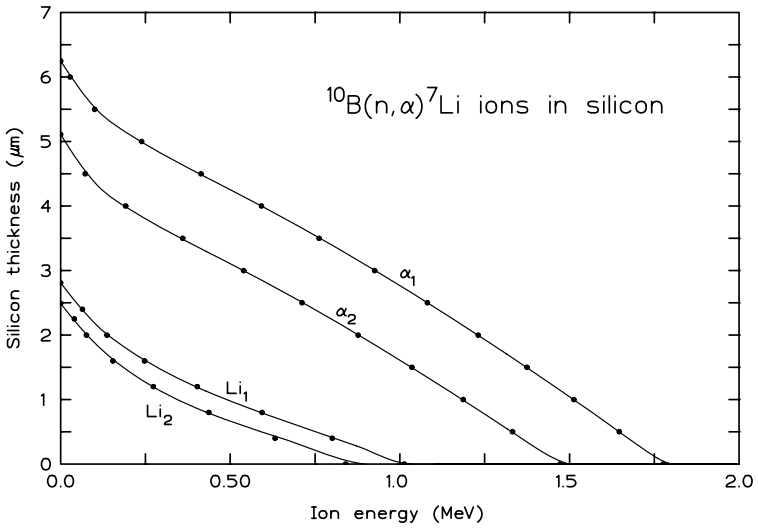

Figure 4. Path length in silicon versus the mean residual energy for the ions produced in the $^{10}\mathrm{B}(n,\alpha)^{7}\mathrm{Li}$ reaction. Circles are data calculated by the TRIM code and lines are the empirical fits of Eq. (4).

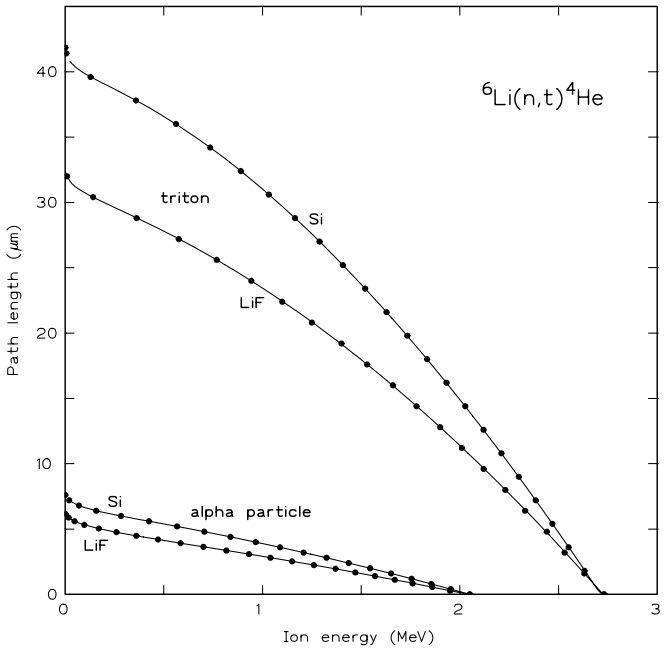

Figure 5. Path length in silicon and LiF versus the mean residual energy for the ions produced in the $^{6}\mathrm{Li}(n,t)^{4}\mathrm{He}$ reaction. Circles are data calculated by the TRIM code and lines are the empirical fits of Eq. (5) and Eq. (6).

TRIM calculations of the energy straggling for the four ions produced in the ^{10}B(n,α)^{7}Li reaction were made and the following empirical equation was fit to the calculated results:

$$\frac{\sigma_{str}}{E} = a + bE^c. \tag{8}$$

The empirical fit and the calculated energy straggling values are shown in Fig. 6. Values of the fitting parameters are given in Table 7.

Table 7. The initial energies, range in silicon, and the fit parameters for Eq. (8) for the ions produced in the ^{10}B(n,α)^{7}Li reaction.

ion	E_o (MeV)	Range (μm)	Parameters for Eq. (8)		
			a	b	c
α_1	1.7762	6.25	−.087053189	0.107157820	−0.37284172
α_2	1.4721	5.11	−.084451428	0.098519784	−0.37706387
Li_1	1.0133	2.81	−.035292668	0.043321774	−0.59331028
Li_2	0.8398	2.49	−.049446492	0.048381691	−0.56563867

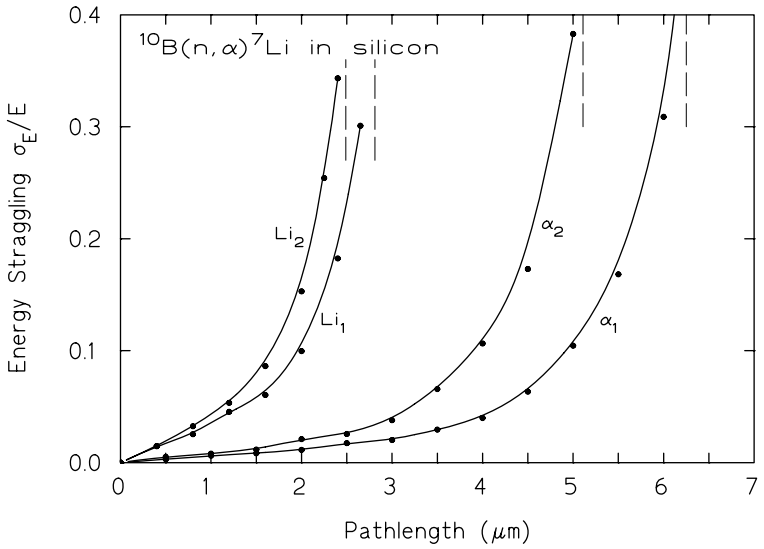

Figure 6. TRIM results for σ_{str}/E (circles) and the empirical fit of Eq. (7) (lines). The vertical dashed lines indicate the range in a silicon of each ion.

2.2 Empirical Results for Lithium Fluoride

The residual energy (MeV) in LiF of the ^{6}Li$(n,t)^{4}$He α particle can be well approximated by Eq. (2). The residual energy of the triton is approximated by Eq. (3). In both approximations x has units of μm. Values for the empirical parameters in these formulas are listed in Table 8 and the approximation is compared to the TRIM data in Fig. 3.

The path length $\overline{X}(E)$ in LiF for reaction ions to reach an energy E (MeV) is approximated by Eq. (5) for the α particle and by Eq. (6) for the triton. Values for the empirical parameters in these formulas are listed in Table 8 and the approximation is compared to the TRIM data in Fig. 5.

Table 8. Values of the parameters for the empirical approximations for the residual energy $\overline{E}(x)$ and the path length to reach energy E, $\overline{X}(E)$, in LiF for the ions produced in the $^6\mathrm{Li}(n,t)^4\mathrm{He}$ reaction.

	$\overline{E}(x)$ (MeV)		$\overline{X}(E)$ (μm)	
Parm	α [Eq. (2)]	triton [Eq. (3)]	α [Eq. (5)]	triton [Eq. (6)]
a	2.045795872242	1.002503409342	6.312636231356	33.054989509315
b	-0.161868152261	-0.043787370382	-3.594256350143	-6.885172032726
c	-0.665680395107	-0.065185375563	1.968648983630	-2.727479733376
d	-0.000407316315	0.000410451552	-1.822537261104	0.312521118012
e	0.054192529543	0.000957069819	0.136384942661	2.194886238813
f	0.001694213790		-0.128391568854	
e			0.037737798916	

2.3 Empirical Results for Boron

The residual energy (MeV) of the $^{10}\mathrm{B}(n,\alpha)^7\mathrm{Li}$ ions in a boron medium of density $\rho = 2.14$ g/cm^3 can be approximated by Eq. (2) in which x is in μm. Values for the empirical parameters in this formula are given in Table 9. This approximation is compared to the TRIM data in Fig. 7.

The path length $\overline{X}(E)$ in boron for $^{10}\mathrm{B}(n,\alpha)^7\mathrm{Li}$ reaction ions to reach an energy E (MeV) can be approximated by

$$\overline{X}(E) = a + bE + cE^2 + dE^3 + e\sqrt{E}. \tag{9}$$

The fit parameters are listed in Table 10, and a comparison between this approximation and the TRIM data used to make the empirical fit is shown in Fig. 8.

Table 9. Values of the parameters for Eq. (2) for the $^{10}\mathrm{B}(n,\alpha)^6\mathrm{Li}$ ions in boron with mass density $\rho = 2.14$ g/cm^3.

Parm	α_1	α_2	Li_1	Li_2
a	1.770161519664	1.464892652938	1.001502185168	0.826861137634
b	-0.247369744654	-0.280020362263	-0.209070917295	-0.214925712448
c	-0.777189670485	-0.788408900360	-0.949487084918	-0.899542069162
d	0.005627752923	0.004982309886	0.092121206407	0.110279421687
e	0.085317374793	0.106062126165	0.224397207451	0.244302839804
f	0.002373340329	0.005899184081	-0.031444715566	-0.070392084014

Table 10. Values of the parameters for Eq. (9) for the $^{10}\mathrm{B}(n,\alpha)^6\mathrm{Li}$ ions in boron with mass density $\rho = 2.14$ g/cm^3.

Parm	α_1	α_2	Li_1	Li_2
a	4.589490452589	3.695907197066	2.036116649701	1.794056712859
b	-0.134954877186	-0.295619764910	-1.123100802529	-1.397105114589
c	-0.665577619347	-0.558554287069	0.843675375487	1.312427235593
d	0.013020747571	-0.022011126975	-0.448338547191	-0.775860695429
e	-1.760545699938	-1.653898062555	-1.311051413201	-1.211961286233

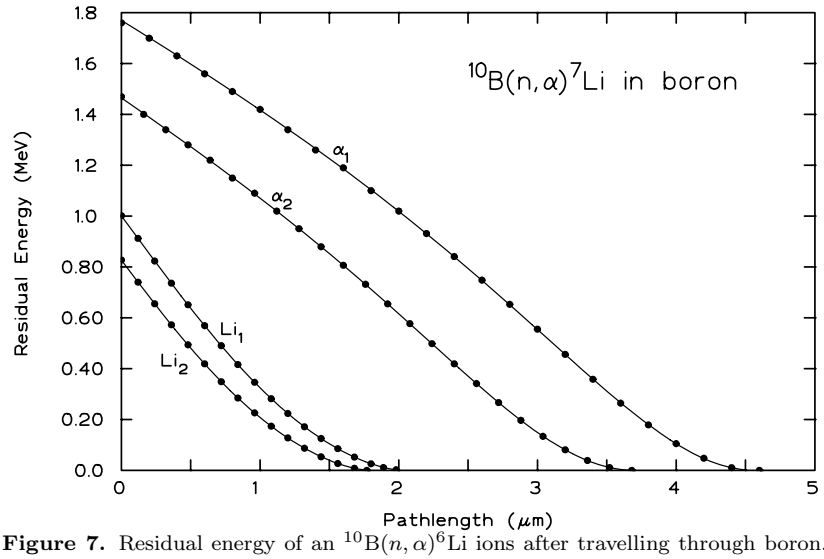

Figure 7. Residual energy of an $^{10}\mathrm{B}(n,\alpha)^{6}\mathrm{Li}$ ions after travelling through boron. Circles are data calculated by the TRIM code and lines are the empirical fits of Eq. (2).

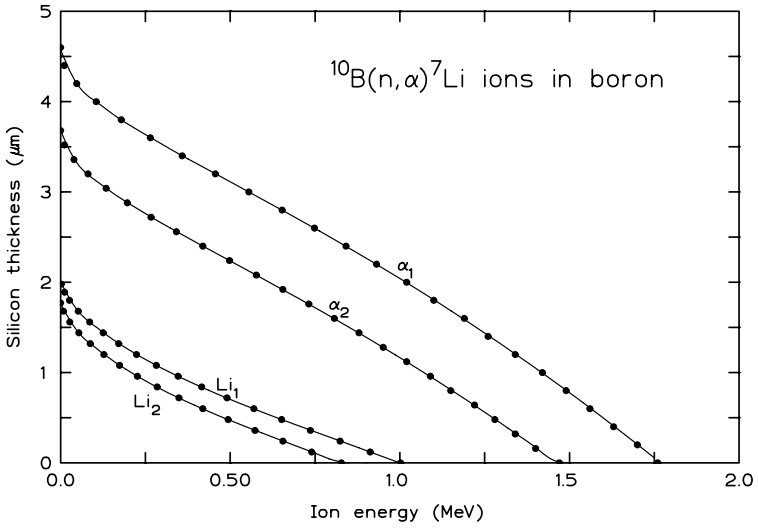

Figure 8. Path length in boron versus the mean residual energy for the ions produced in the $^{10}\mathrm{B}(n,\alpha)^{7}\mathrm{Li}$ reaction. Circles are data calculated by the TRIM code and lines are the empirical fits of Eq. (4).

3 A Monte Carlo Approach for Estimating Ion Spectra

The Monte Carlo technique can be applied with great effectiveness to determine the spectrum of energies deposited by reaction ions in a material as they slow through it, giving up their kinetic energy by ionizing and exciting the ambient atoms. Such spectral calculations are needed for the interpretation of ion deposition spectra measured by neutron depth profiling (NDP). The application of Monte Carlo to NDP is reported elsewhere [Shultis 2003, 2004]. In this report the Monte Carlo method is applied to the evaluation of various designs for semiconductor detectors.

3.1 Description of the Monte Carlo Simulation

3.1.1 Simulation of Neutron Interactions in Semiconductor Detector

In these simulations, a plane parallel beam is assumed to uniformly illuminate the detector. The silicon semiconductor is assumed transparent to these neutrons and the total cross section for the converter material (LiF or boron) is taken as the ion-producing cross section. Neutron scattering effects are not considered.

By sampling uniformly over the illuminated surface of the detector, a random point (x_i, y_i) for neutron entry on the detector surface is determined. Then along a ray through this entry point, a random depth z_i for a neutron interaction in the converter material is obtained by sampling from the distribution $f(z_i) = C\exp(-\Sigma_c z_i)$ where Σ_c is the thermal average macroscopic cross section for the converter material. Here $C = [1 - \exp(-\Sigma_c T)]^{-1}$ is a normalization constant to make $f(z)$ a properly normalized probability distribution function (pdf). The depth T is the length of the ray through the converter material. If no converter material is in the path of the neutron ray ($T = 0$) then the neutron passes through the detector without interaction.

Once a random interaction site (x_i, y_i, z_i) is determined, a random direction $\mathbf{\Omega}_i = (u_i, v_i, w_i)$, where (u_i, v_i, w_i) are the directed cosines for $\mathbf{\Omega}$, for one of the ions is selected from and isotropic directional distribution. The other reaction ion is then given the opposite direction $(-u_i, -v_i, -w_i)$. Finally, the identity of the ions is randomly selected according to the branching ratio of the various ions produced in the neutron interaction. The two ions are then tracked along their paths in the detector, and the energy transferred to the silicon regions estimated.

3.1.2 Energy Deposition in Semiconductor Detectors

The estimation of the energy deposited in various regions of a silicon semiconductor detector by ions produced by thermal neutron reactions in adjacent regions of boron or lithium fluoride is greatly simplified if all ions are assumed to travel in straight lines, i.e., scattering events and energy straggling can be neglected. Then calculating the energy deposited in the various regions of the detector is simply a matter of calculating the length of the geometric segments an ion travels in each material encountered along its straight-line path from the ion's point of birth to where it is stopped. The energy deposited in the silicon by each simulated ion history is then found by calculating the energy lost by the ion over every path segment it travels through the silicon.

To calculate the energy lost by an ion over each of its path segments, two empirical functions are needed. The first $\overline{E}^i_m(x)$ is the mean residual energy after an ion of type i travels a distance x in material m. To obtain this function, the TRIM code [Ziegler, 2001] was used to obtain a tabulation of the mean residual energy of the various ions produced by thermal neutron interactions in the converter material (LiF or boron) as a function of path length in the converted material and in silicon. Then the TableCurve [Jandel 1996] computer program was used to fit thousands of different functions to these data. In this way accurate empirical formulas were found for $E^i_m(x)$ that

permitted rapid evaluation of an ion's residual energy. These empirical formulas are presented in Section 2.

The second function needed for the Monte Carlo calculations is $\overline{X}^i_m(E)$, which is the path length in material m for the ith ion to obtain a mean residual energy E. This function is the inverse of $E^i_m(x)$. Again, empirical fits to $X^i_m(E)$ were also obtained and are presented in Section 2. The function $\overline{X}^i_m(E)$ also gives the mean range of the ith ion in material m, namely $R^i_m = \overline{X}^i_m(0)$. With these two empirical fits for $\overline{E}^i_m(x)$ and $\overline{X}^i_m(E)$, the energy deposited by an ion along any straight-line segment in any of the detector regions can readily be obtained.

Consider an ion that leaves a region composed of material 1 with energy E_1 and enters an adjacent region composed of material 2. The ray in the direction of the ion travel is assumed to have a segment length s_2 in the second region, i.e., the distance from the point where the ion enters the second region to the point where the ray intersects another region, the detector boundary, or is stopped. The problem is to estimate the energy deposited along s_2 and the residual ion energy E_2 (if any) at the end of its path in the second region. Clearly, if the ion with an initial energy E_1 in material 2 has a range less than x_2, the energy deposited in the second region is $E_d = E_1$ since $E_2 = 0$. However, if this range is greater that x_2, then $E_2 > 0$ and the deposited energy is $E_d = E_1 - E_2$.

To calculate E_2 at end of the ray in the second medium, we first backtrack the trajectory to find the ion's starting position, *if the first medium were replaced by the second medium*, to produce the same residual energy at the interface. This back-tracked distance is $x_1 = \overline{X}^i_2(E_1)$. The energy E_2 after a path length $x_1 + x_2$, all in the material of medium 2, is simply $E_2 = \overline{E}^1_2(x_1 + x_2)$. In this manner the energy deposited along any ion track segment can be readily evaluated.

The energy the two reaction ions deposit in the silicon regions along their tracks is then recorded in an appropriate bin or tally vector for each simulated reaction event. After performing this simulation for several million reactions, an ideal energy-deposition spectrum in thus obtained.

3.1.3 Simulated Measured Energy-Deposition Spectra

The spectra obtained by Monte Carlo simulations are ideal in the sense that no energy straggling, large-angle ion scattering or detector noise and resolution effects are considered. To simulate expected multi-channel analyzer measured spectra, which include such non-ideal effects, the ideal spectra are post processed to introduce a Gaussian averaging or smearing of the counts in each energy bin of the ideal spectra.

Let $P(E)dE$ be the probability a neutron reaction leads to the deposition of energy in dE about E. The number of counts N_i in channel i of the ideal spectrum is

$$N_i = N_{tot} \int_{E_i-\Delta}^{E_i+\Delta} P(E)\, dE \simeq 2\Delta\, N_{tot} P(E_i), \tag{10}$$

where E_i is the channel midpoint energy, 2Δ is the bin energy width, and N_{tot} is the total number of neutron reactions. Because of non-ideal effects, an energy deposition of E has a probability $\Re(E, E')dE'$ of being recorded in dE' about E'. To a first approximation, a Gaussian resolution function is assumed, i.e.,

$$\Re(E, E') = \frac{1}{\sqrt{2\pi}\sigma} \exp\left[-\frac{1}{2}\left(\frac{E - E'}{\sigma}\right)^2\right]. \tag{11}$$

The probability a reaction that deposits energy in dE about E and is then recorded in channel j of

the MCA spectrum is thus

$$C_j(E)dE = P(E)dE \int_{E_j-\Delta}^{E_j+\Delta} \Re(E, E')\, dE', \tag{12}$$

so that the number of counts in channel j of the measured spectrum is

$$\begin{aligned}
\widehat{N}_j &= N_{tot} \int_0^{E_{\max}} C_j(E)\, dE \\
&= N_{tot} \int_0^{E_{\max}} P(E) \left[\int_{E_j-\Delta}^{E_j+\Delta} \Re(E, E')\, dE' \right] dE \\
&\simeq N_{tot} \sum_{i=1}^{N_{\max}} P(E_i) 2\Delta \left[\int_{E_j-\Delta}^{E_j+\Delta} \Re(E_i, E')\, dE' \right] \\
&= \sum_{i=1}^{N_{\max}} N_i W_{ij},
\end{aligned} \tag{13}$$

where $E_{\max}$ is the maximum spectral energy, $N_{\max}$ is the maximum number of MCA energy bins, and the *spreading vector* is

$$\begin{aligned}
W_{ij} = W_{ji} = W_{|i-j|} &= \frac{1}{\sqrt{2\pi}\sigma} \int_{E_j-\Delta}^{E_j+\Delta} \exp\left[-\frac{1}{2} \left(\frac{E_i - E'}{\sigma} \right)^2 \right] dE' \\
&= \frac{1}{2} \left\{ \operatorname{erf}\left(\frac{E_j + \Delta - E_i}{\sqrt{2}\sigma} \right) - \operatorname{erf}\left(\frac{E_j - \Delta - E_i}{\sqrt{2}\sigma} \right) \right\}.
\end{aligned} \tag{14}$$

For the simulated spectra shown in this report, a standard deviation of $\sigma = 20$ keV, typical of silicon detectors, is assumed.

3.2 Estimation of the Detector Efficiency

In this study, the Monte Carlo simulation method described above was used to estimate the overall thermal-neutron detector efficiency. This is defined as the fraction of all thermal neutrons incident on the detector that interact in the converter material and whose subsequent ions deposit at least some minimal amount of energy, E_{cut}, in the silicon on the detector. In these simulations, a single tally bin was used to record such interactions, so that the detector efficiency could be estimated without the extra expensive of summing the simulated spectra to find the number of histories that deposited more than E_{cut} in the silicon. This number divided by the total number of histories gives the detector efficiency ϵ.

Closely related to the efficiency of the detector is $P_{(n,x)}$ defined as the fraction of the incident neutrons that cause an (n, x) reaction, in which x represents the lighter of the two product ions. For ^{10}B and ^{6}LiF, $\Sigma_c \simeq \Sigma_{(n,x)}$, so that $P_{(n,x)}$ also is the fraction of the incident neutrons stopped in the detector or the *stopping fraction*. This quantity, which is usually easy to calculated analytically from the detector geometry, is an upper bound to the detector efficiency, i.e., $\epsilon \leq P_{(n,x)}$. Moreover, in the limit of very small detectors (compared to the ion ranges), all ions can escape the converter regions and deposit an energy greater than E_{cut}. Hence, the detector efficiency can be expected to approach $P_{(n,x)}$ as the detectors become smaller. This limiting case can therefore be used as a verification check for Monte Carlo simulations.

4 Film-Coated Semiconductors

The simplest thermal-neutron semiconductor detector is a semiconductor whose surface is coated with a thin film of converter material such as ^{10}B or ^{6}LiF. In such a device, one of the two reaction ions is emitted towards the semiconductor while the other, emitted in the opposite direction, has no chance of being detected. Clearly there is an optimum coating thickness. If too small, few incident neutrons interact in the converter material. If too thick, reaction ions are stopped in the film and never reach the semiconductor detector. To increase the efficiency of such detectors, two coated semiconductor detectors can be placed back-to-back (i.e., the coated surfaces are placed together. In such a "sandwich detector" both ions born in the converter film have a chance of being detected.

To estimate the optimum film thickness of a sandwich detector, an infinite horizontal slab of converter material in an infinite medium of a silicon semiconductor was considered. In a Monte Carlo simulation, thermal neutrons (a Maxwellian spectrum at room temperature) were assumed to be normally incident on the converter film. Again there should be a film thickness that maximizes the detector efficiency. Too thin a film allows neutron to be transmitted without interacting. while too thick a film prevents reaction ions from reaching the semiconductor detector. For this detector, the stopping fraction, i.e., the probability a neutron causes an ion-producing reaction, is simply

$$P_{(n,x)} = 1 - \exp(-\Sigma_c t), \tag{15}$$

where t is the thickness of the converter film.

Monte Carlo estimated detection efficiencies for ^{10}B and ^{6}LiF converter materials are shown in Figs. 9 and 10, respectively, as a function of the converter thickness. In these figures, P_n^{up} and P_n^{dn} are the probabilities that the reaction ions are detected in the upper semiconductor (the one the upon which the neutrons are incident) and the lower semiconductor, respectively. These results are in agreement with those obtained by McGregor et al. [2003] who, for the simple geometry of this problem, used analytic results for the detector efficiency as a function of film thickness. Notice, that for ^{10}B the maximum efficiency is about 8.3% for 3.5 μm converter thickness, while in ^{6}LiF it is about 7.9% for a 35 μm thickness. Finally, as expected, as the film thickness becomes very small, the detector efficiency approaches $P_{(n,x)}$.

The signature of a thermal-neutron semiconductor detector is the distribution of ions energies recorded by the detector [McGregor and Shultis, 2004]. In Fig. 11 the energy deposition spectrum of ions recorded in a sandwich thin-film semiconductor detector is shown along with the components of the energy deposited in the lower and upper detectors. Similar spectra are shown in Fig. 12 for ^{6}Li. Both of these figures are for film thicknesses that maximum the thermal-neutron detection efficiencies. The "edges" in these spectra correspond to the maximum energies of the ions produced by the thermal-neutron reactions. Also to be noted is that the upper semiconductor (through which the neutrons pass to reach the converter material) is slightly more efficient at detecting neutrons than is the lower semiconductor detector. This again agrees with observations made by McGregor et al. [2003].

5 Stacked Slabs of Silicon and Converter

To increase the detection efficiency for thermal neutrons, a series of sandwich detectors, each with a slab of converter material, could be stacked atop one another and exposed edge-on to the neutron beam. Neutrons entering the converter material can thus be totally absorbed and, if the converter slab is sufficiently thin, one or both reaction ions enter the semiconductor and be recorded. However, neutrons entering the silicon will be transmitted without interaction. Thus, the relative widths of the silicon and converter regions strongly affect the detection efficiency of such a stacked semiconductor detector. Such stacked arrays can be formed by etching very deep channels into the semiconductor material and then filling the channels with the ^{10}B or ^{6}Li converter (see Fig. 13).

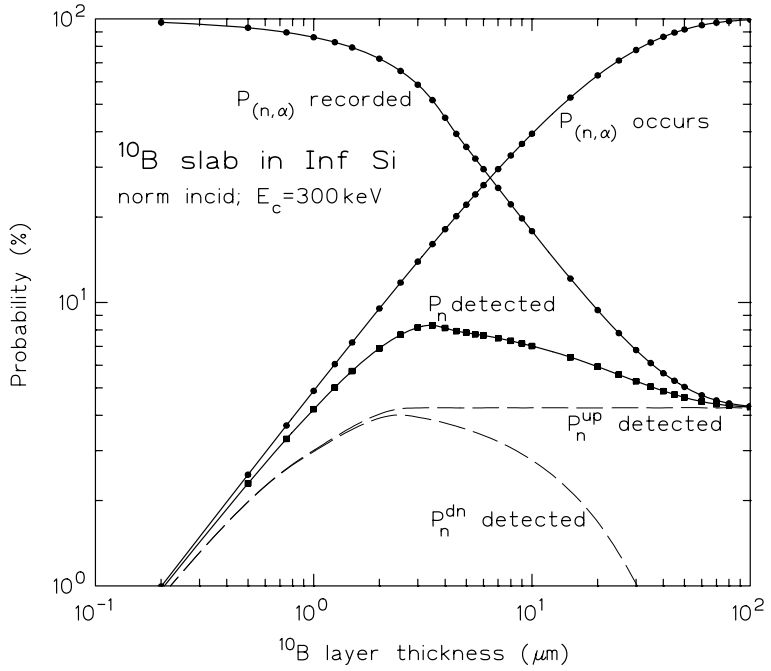

Figure 9. Thermal-neutron detection efficiency of a "sandwich" semiconductor detector with ^{10}B as the converter material as a function of the converter thickness.

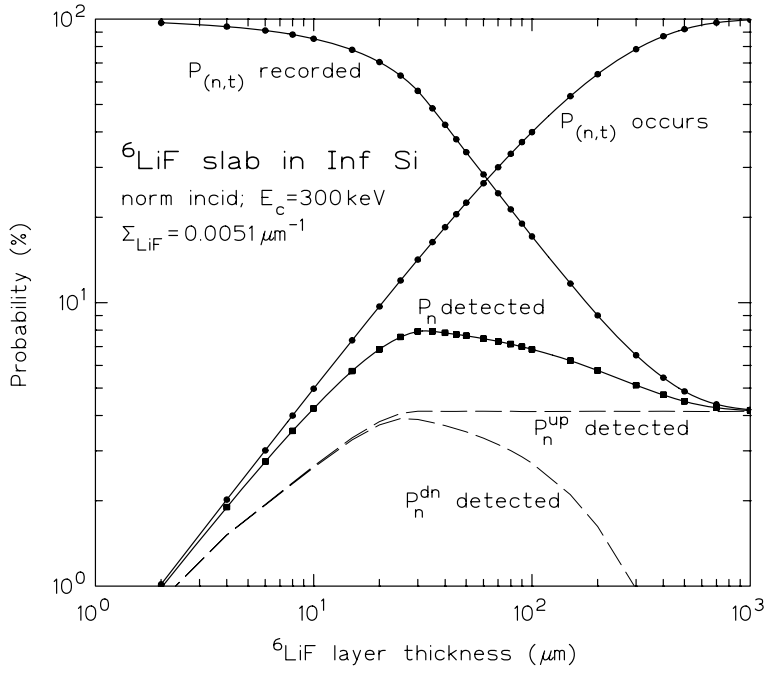

Figure 10. Thermal-neutron detection efficiency of a "sandwich" semiconductor detector with ^{6}LiF as the converter material as a function of the converter thickness.

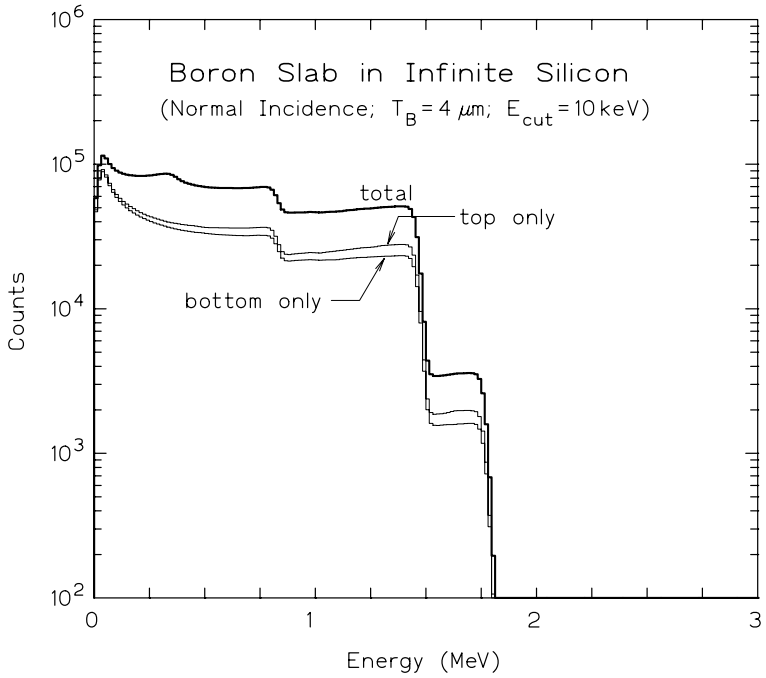

Figure 11. Ion energy deposition in a ^{10}B sandwich detector.

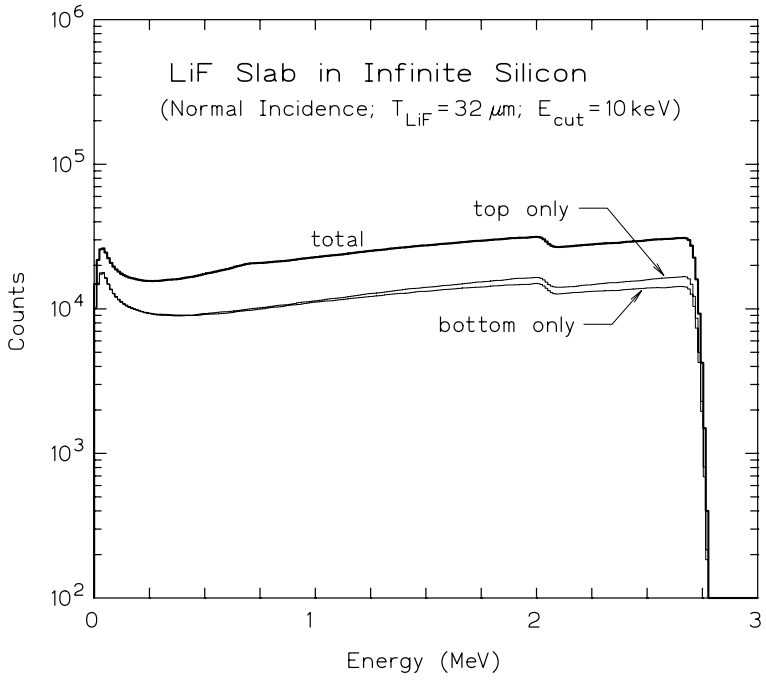

Figure 12. Ion energy deposition in a ^{6}LiF sandwich detector.

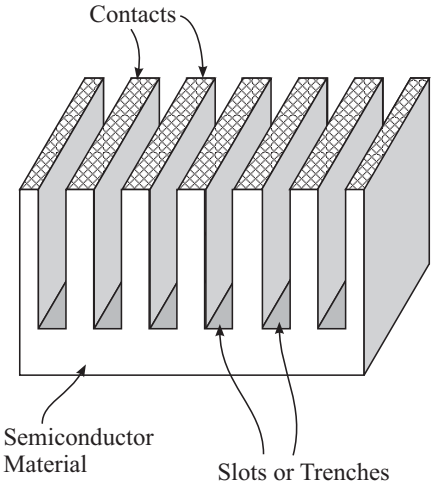

Figure 13. Channels etched into silicon used to form a stack of sandwich detectors.

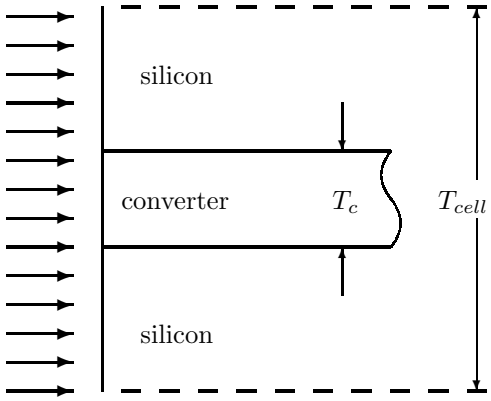

Figure 14. Neutrons incident on the side of a unit cell containing an infinite slab of converter material.

Consider the unit cell of a stack of alternating layers of converter and semiconductor shown Fig. 14. In this section the channel is assumed to be infinitely deep. The cell has width T_{cell} and the infinite converter slab (channel) width is T_c. In the energy-deposition calculations, it was assumed that the thickness of silicon on either side of the converter slab $T_{cell} - T_c$ is greater than the range of the reaction ions. In Figs. 15 and 16 ion energy-deposition spectra in the silicon for ^{10}B and ^{6}LiF converter materials, respectively, are shown as a function of the converter slab thickness. For thin converter slabs, both reaction ions can reach the semiconductor and, consequently, energy up to the Q-value of the reaction can be deposited in the silicon. However, for a thick converter slab, only one ion reaches the silicon and the energy-deposition spectrum becomes that of a coated semiconductor detector (see Figs. 11 and 12).

Clearly, to increase the detector efficiency of a stacked array, the amount of silicon, through which the neutrons stream without detection, should be minimized. However, the thickness of the silicon layers, $T_{cell} - T_c$, must be sufficiently thick to absorbed energy above E_{cut} of the ions born near the surface of the converter slab. For this detector geometry, the probability an incident neutron causes an ion-producing reaction is simply $P_{(n,x)} = T_c/T_{cell}$ since any neutron incident on the infinite converted slab is absorbed.

With stacked array detectors, detection efficiencies much greater than those of film coated detectors can be realized. Thermal neutron detection efficiencies for such stacked arrays, when irradiated end-on (see Fig. 14), are shown in Figs. 17 and 18 for different cell thicknesses T_{cell}. Again, as the converter region becomes very small, the Monte Carlo calculated detector efficiency approaches the stopping fraction $P_{(n,x)}$.

Although the highest efficiencies are realized for very small cell widths, fabrication considerations limit how small a cell can be made and how deep a channel can be etched into the silicon. However, a unit cell with an infinite converter slab when irradiated end-on is four to five times more efficient than if the cell were irradiated normally to the converter layer (compare the results of Figs. 14 and 17 to those of Figs. 9 and 10).

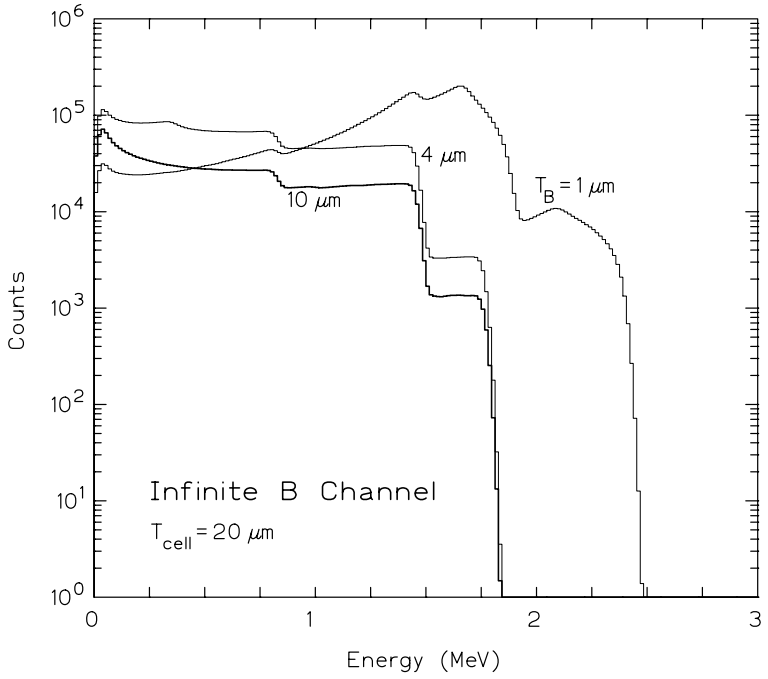

Figure 15. Ion energy deposition in a set of stacked infinite layers of ^{10}B and silicon.

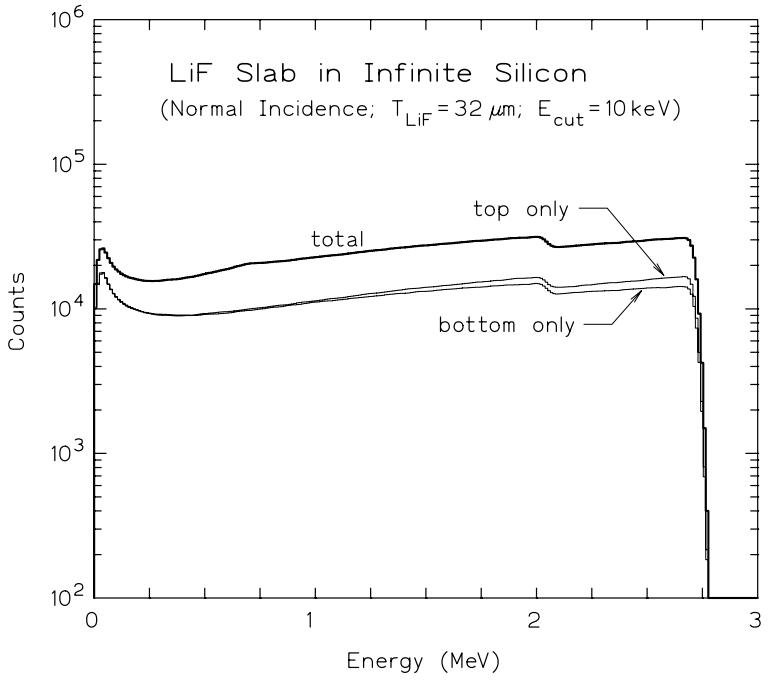

Figure 16. Ion energy deposition in a set of stacked infinite layers of ^{6}Li and silicon.

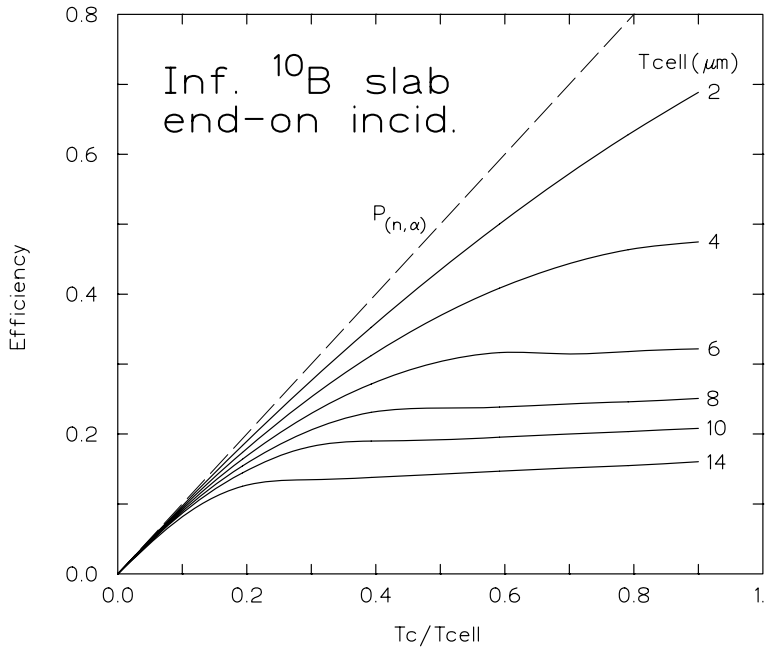

Figure 17. Estimated thermal-neutron detector efficiencies for stacked layers of ^{10}B and silicon of different thicknesses for E_{cut} = 300 keV. Irradiation is normal to the edge of the boron-silicon cell. Neutrons are uniformly incident parallel to the converter layers

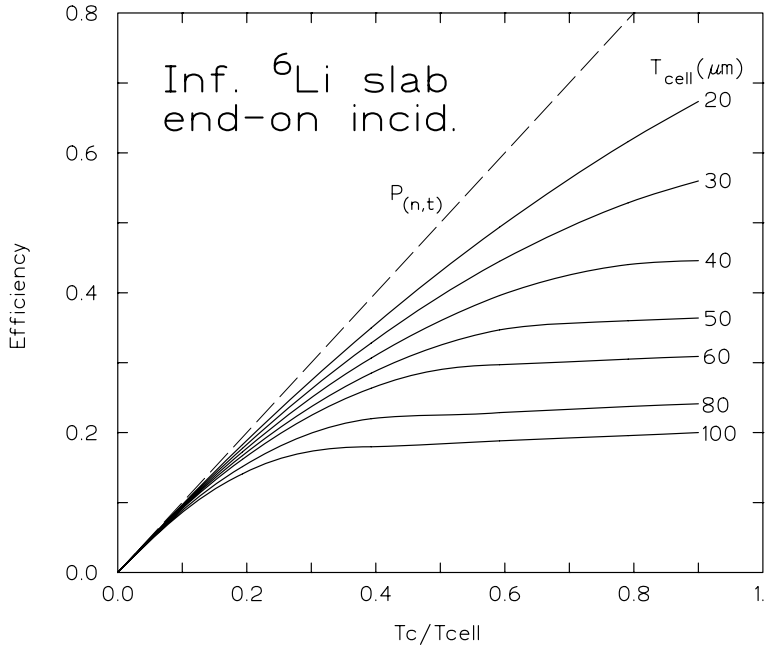

Figure 18. Estimated thermal-neutron detector efficiencies for stacked layers of ^{6}Li and silicon of different thicknesses for E_{cut} = 300 keV. Irradiation is normal to the edge of the lithium-silicon cell. Neutrons are uniformly incident parallel to the converter layers

6 Semiconductor Detectors with Cap and Internal Channels

An alternative design for a semiconductor detector is shown in Fig. 19. In this device a series of rectangular channels of width T_{wall} and depth H_{wall} is etched into the silicon semiconductor and filled with a converter material. In addition, a film or cap of the same converter material is placed over the top of the device. The thickness of this cap is denoted by T_{cap} and the width of the unit cell, shown in Fig. 19, by W_{cell}. A Monte Carlo simulation code was written to estimate the distribution of energy deposited by ions in the semiconductor by ions created by neutron reactions in the converter regions. Two irradiation geometries are considered. In the first (*cap incidence*), the neutrons are uniformly and normally incident on the cap. In the second (*reverse incidence*), neutrons are uniformly and normally incident on the semiconductor surface opposite the cap (the bottom surface in Fig. 19.

In this semiconductor detector there are 6 distinct straight-line ion trajectories that can lead to energy being deposited in the semiconductor (see Fig. 20). In a type 1 event, an ion born in the cap heads toward the silicon and away from the wall. The second ion, emitted in the opposite direction, heads away from the silicon and, thus, can deposit no energy in the silicon. In a type 2 event, an ion born in the cap heads toward the silicon and the channel wall. The second ion heads away from the silicon. In a type 3 event, an ion born in the cap first enters the wall before heading towards the silicon. The second ion contributes nothing. In a type 4 event, ions are born in the wall below the cap and only the downward ion heads towards the silicon. In a type 5 event, ions are born in the wall below the cap and both head towards the silicon. Both ions can thus deposit energy in the silicon. In a type 6 event, ions are born in the cap above the channel and, thus, only the downward ion can possibly reach the silicon.

In Figs. 21 and 22 examples of the ion-deposition energy spectra are shown for a semiconductor detector based on ^{6}LiF. Figures 23 and 24 give similar results for a semiconductor detector based on ^{10}B. The maximum energy that can be deposited in the silicon is the Q-value for the ^{10}B (n, α) reaction (2.79 MeV) or for the ^{6}Li (n, t) reaction (4.78 MeV). Such full energy events can be produced only by reactions near the bottom of the channel and where both reaction ions can escape into the silicon with negligible energy loss while escaping the converter material (trajectory type 5). In all

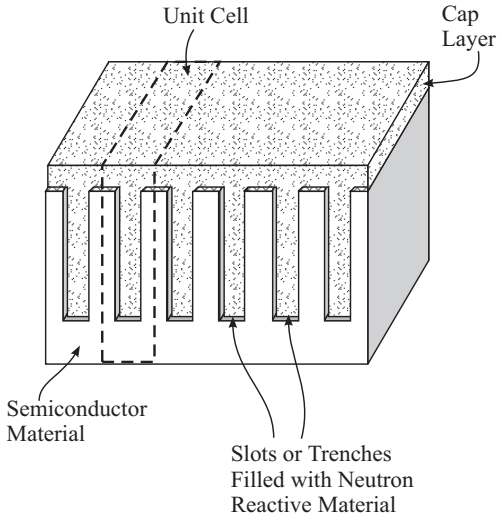

Figure 19. A semiconductor detector composed of infinitely long channels filled with ^{10}B or ^{6}Li and a cap composed of the same converter.

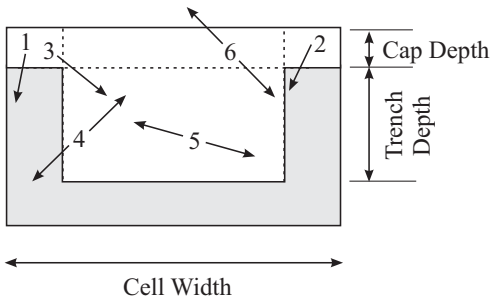

Figure 20. The 6 possible types of ion trajectories that must be considered for energy-deposition in the semiconductor.

other trajectory types, only a single ion can reach the silicon so that the maximum energy deposited can be no more than the most energetic ion (2.73 MeV for the ^{6}Li reaction and 1.77 MeV for the ^{10}B reaction. Other features in these energy deposition spectra are readily identified in terms of the energies of the other reaction ions.

In Figs. 22 and 24 it is seen that the incident direction of the neutron beam affects the energy deposition spectrum. A detector normally illuminated on the surface opposite the converter cap has a slightly greater efficiency than if the cap were normally illuminated. The greatest production rate of ions in the channel occurs in the region closest to the incident beam. When the bottom of the channel is the incident surface one of the pair of ions produced has a good chance of entering the silicon since any ion emitted in the direction of the beam will enter the silicon. By contrast, if the cap end of the channel is illuminated, ions produced in the channel cannot reach silicon if they are emitted in the direction of the incoming neutrons. In effect the cap acts as an absorber for ions produced in the channel just beneath the cap.

6.1 Efficiency of a Semiconductor Detector with Cap and Channels

Extensive simulations were performed to estimate how the efficiency of a semiconductor detector with a cap and channels of converter material varies with the cell dimensions. Compilations of the results are presented in the Appendix in Tables A.1 to A.4. Some representative graphs constructed from data in the tables are shown in Figs. 25 and 26 for ^{6}LiF as the converter and in Figs. 27 to 32 for ^{10}B as the converter. For all these calculations, a discriminator level for the cut-off energy was taken as 300 keV.

For the geometry of the cap plus channel detector, the stopping fraction is

$$P_{(n,x)} = [1 - \exp(-\Sigma_c T_{cap})] + \frac{T_{wall}}{W_{cell}}[1 - \exp(-\Sigma_c H_{wall})].$$

For the ^{6}LiF case with $H_{wall} = 300\mu$m (1.5 mean-free-path lengths) and $T_{wall}/W_{cell} = 0.5$, $P_{(n,t)} = 0.388$. This value serves as an upper bound for the efficiencies of a capless detector shown in Figs. 25 and 26. If the channel were infinitely deep the stopping fraction increases to 0.5 (all neutrons incident on the channel are stopped).

Generally, the smaller the unit cell width and the greater the channel width, the greater is the detector efficiency. There is also an optimum cap thickness beyond which the detector efficiency decreases. Also, illuminating the semiconductor detector on the opposite side of the cap (reverse incidence) increases the efficiency by a few percentage points. As found the Table A.1, the maximum efficiency for a 20 μm ^{6}LiF cell with $T_{wall}/W_{cell} = 0.5$ is 0.333 for a cap thickness of $T_{cap} = 10\mu$m. From Table A.2, for reverse incidence, the maximum efficiency is 0.356 for a cap thickness of $T_{cap} = 20\mu$m.

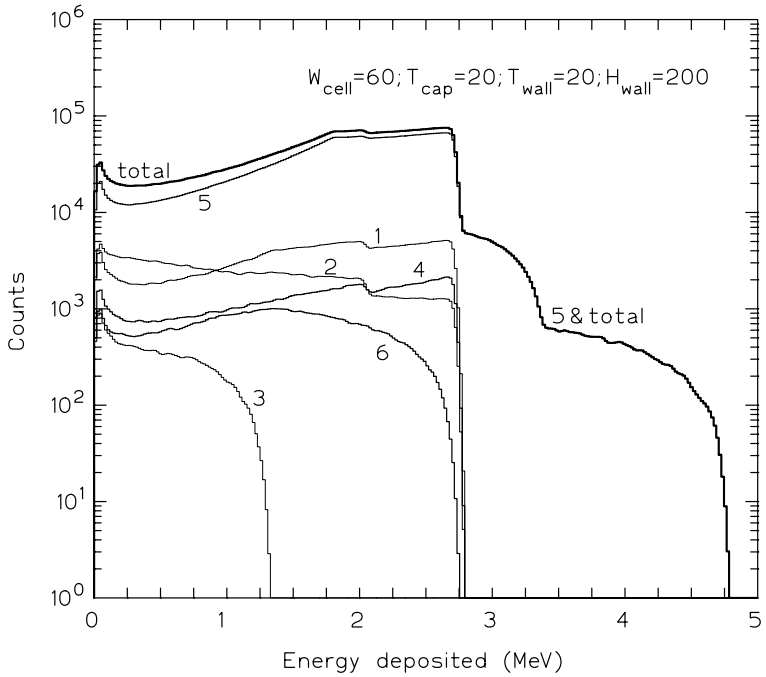

Figure 21. Calculated energy deposition spectrum (heavy line) for a semiconductor detector with rectangular channels and cap of ^{6}LiF. Light lines show the various contributions made by the 6 possible trajectories. Neutrons are normally incident on the cap.

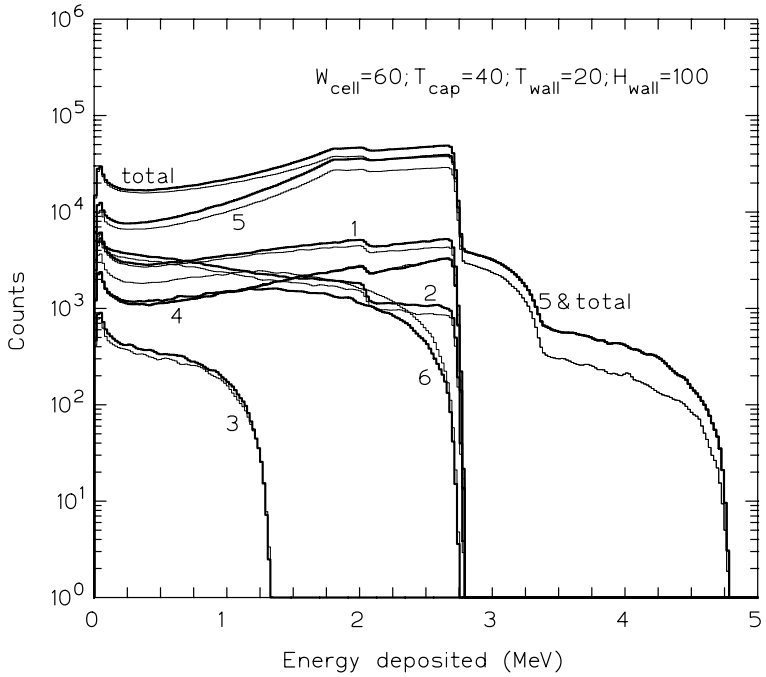

Figure 22. Energy deposition spectrum and the 6 components for a semiconductor detector with rectangular channels and cap of ^{6}LiF. Heavy lines are for neutrons normally incident on the cap and the light lines are for neutrons normally incident in the opposite direction.

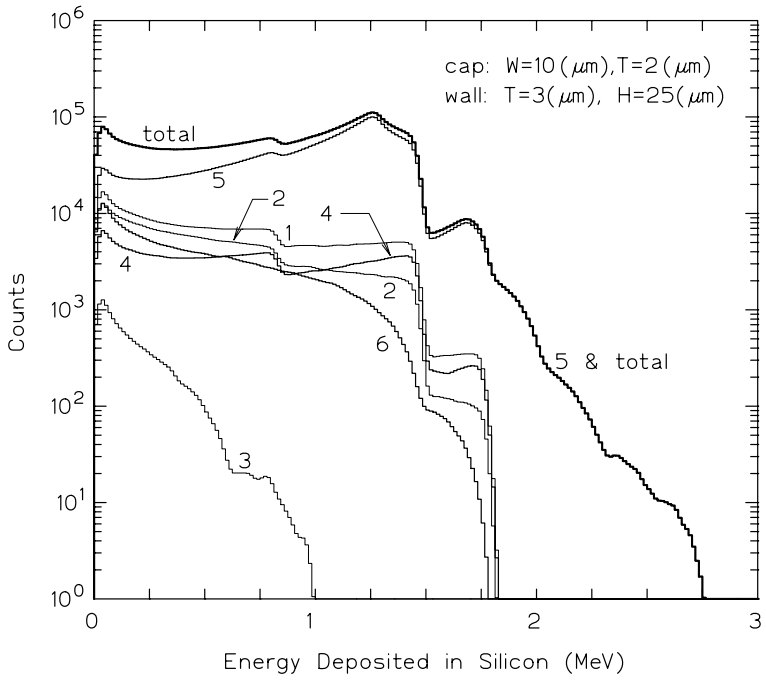

Figure 23. Calculated energy deposition spectrum (heavy line) for a semiconductor detector with rectangular channels and cap of ^{10}B. Light lines show the various contributions made by the 6 possible ion trajectories. Neutrons are normally incident on the cap.

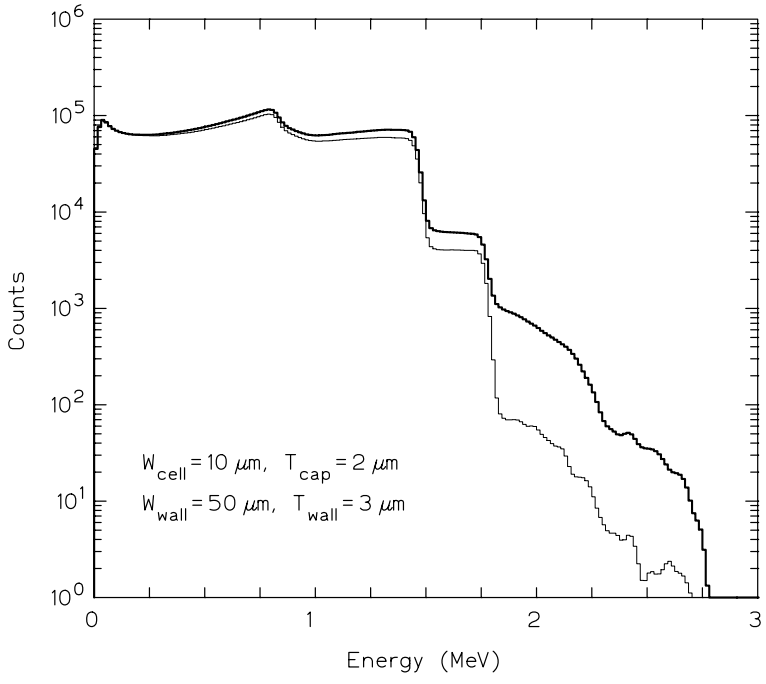

Figure 24. Energy deposition spectrum and the 6 components for a semiconductor detector with rectangular channels and cap of ^{10}B. Light line is for neutrons normally incident on the cap and the dark line are for neutrons normally incident in the opposite direction.

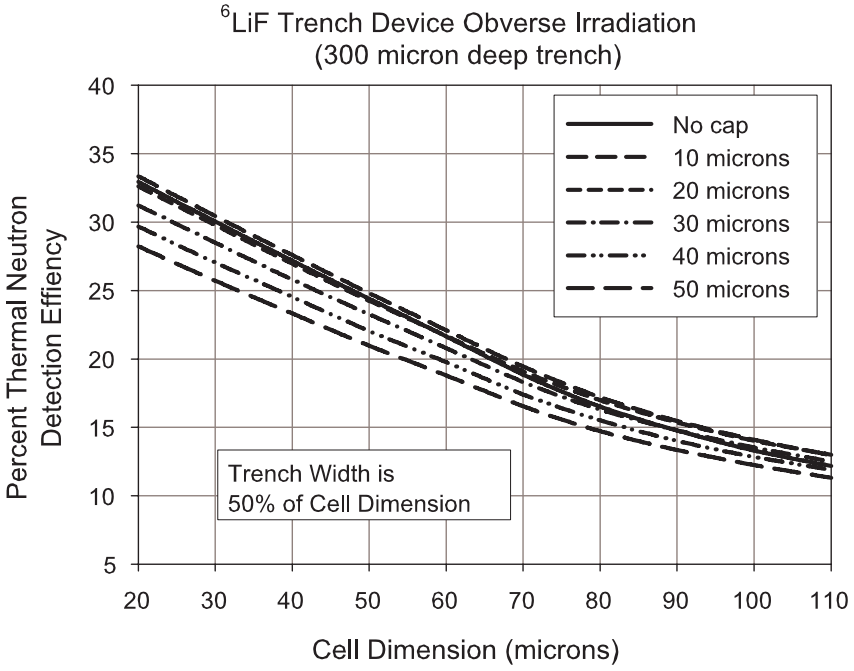

Figure 25. Detector efficiency for 300 μm deep channels filled with ^{6}LiF for various unit cell widths and thicknesses of the ^{6}LiF cap. The width of the trench is one-half of the unit cell width. Neutrons are normally incident on the cap

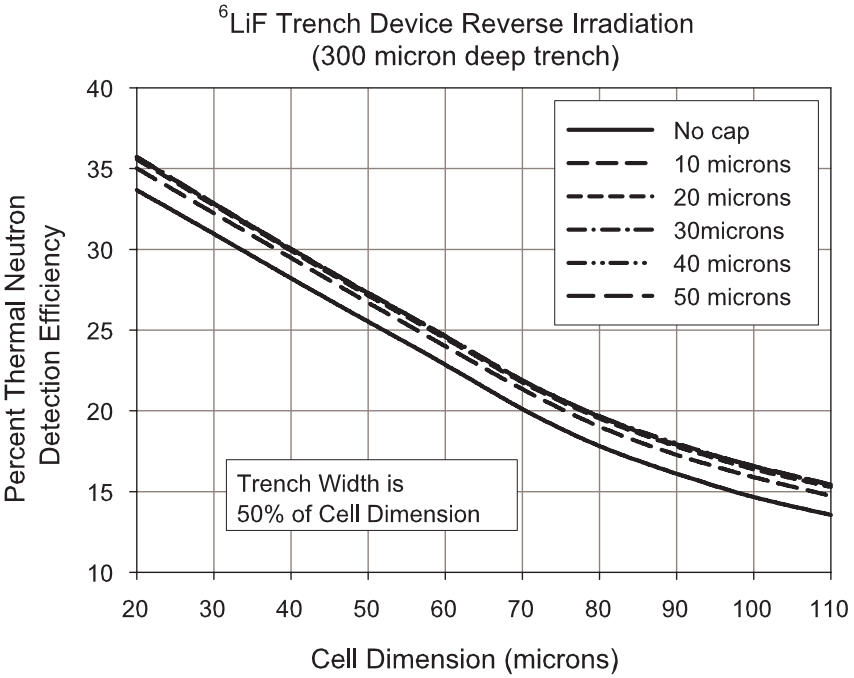

Figure 26. Detector efficiency for 300 μm deep channels filled with ^{6}LiF for various unit cell widths and thicknesses of the ^{6}LiF cap. The width of the trench is one-half of the unit cell width. Neutrons are normally incident on the surface opposite the cap.

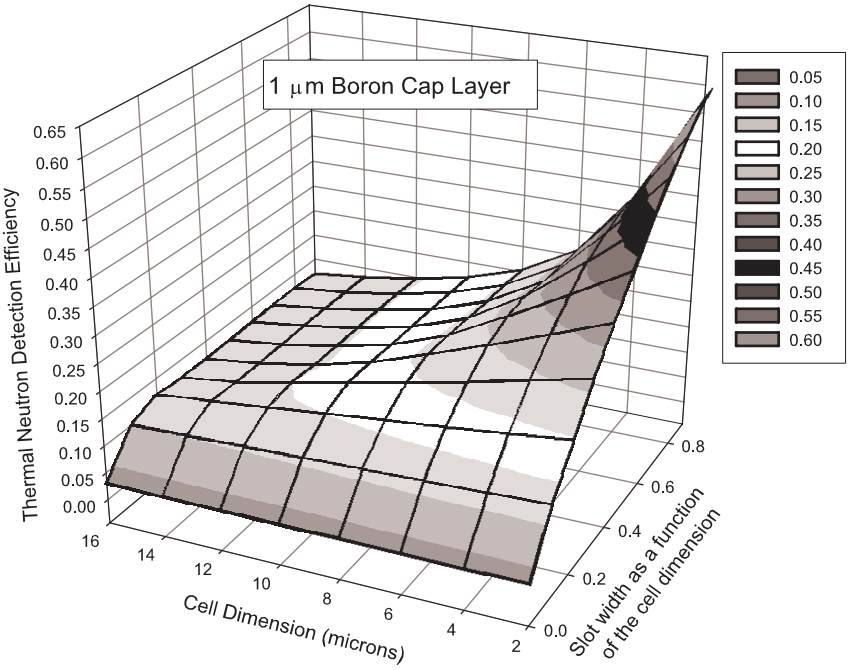

Figure 27. Detector efficiency for 50 μm deep channels filled with ^{10}B and with a 1 μm ^{10}B cap. Neutrons are normally incident on the cap

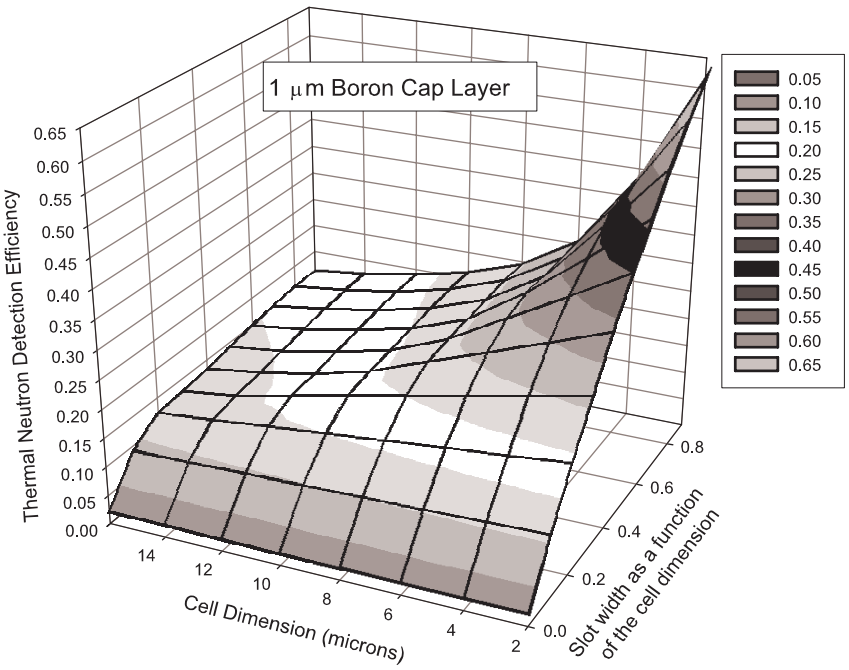

Figure 28. Detector efficiency for 50 μm deep channels filled with ^{10}B and with a 1 μm ^{10}B cap. Neutrons are normally incident on the surface opposite the cap.

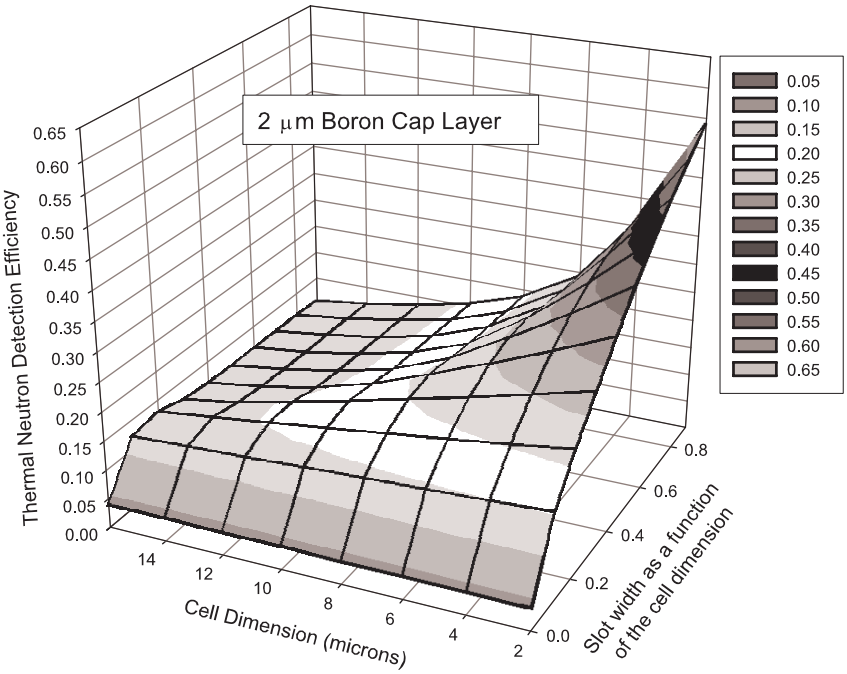

Figure 29. Detector efficiency for 50 μm deep channels filled with ^{10}B and with a 2 μm ^{10}B cap. Neutrons are normally incident on the cap

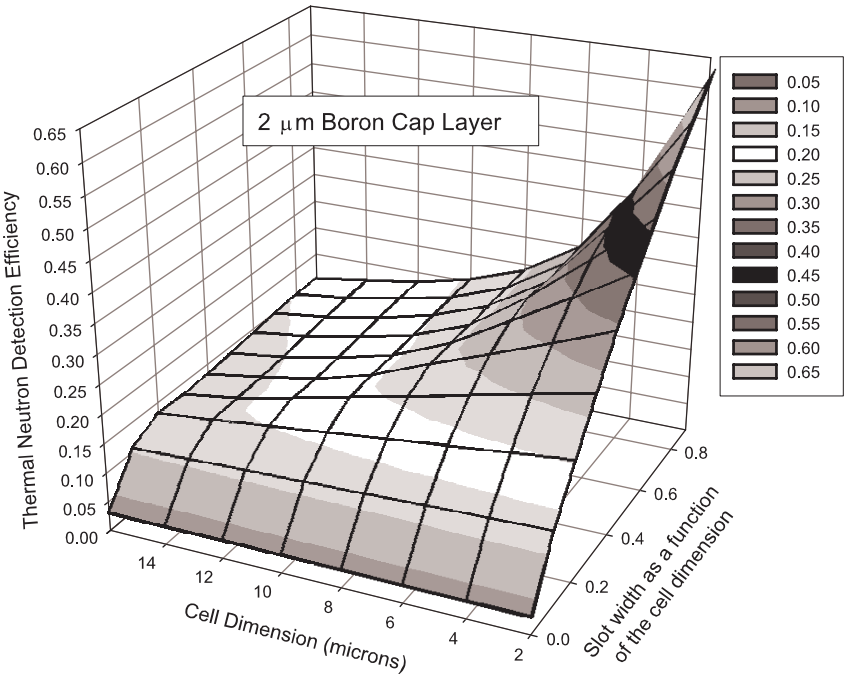

Figure 30. Detector efficiency for 50 μm deep channels filled with ^{10}B and with a 2 μm ^{10}B cap. Neutrons are normally incident on the surface opposite the cap.

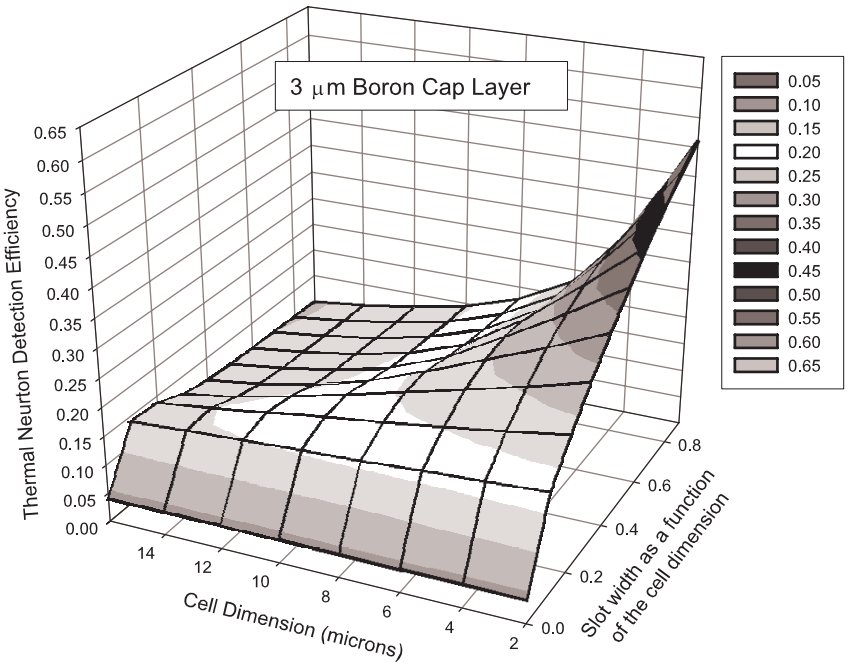

Figure 31. Detector efficiency for 50 μm deep channels filled with ^{10}B and with a 3 μm ^{10}B cap. Neutrons are normally incident on the cap

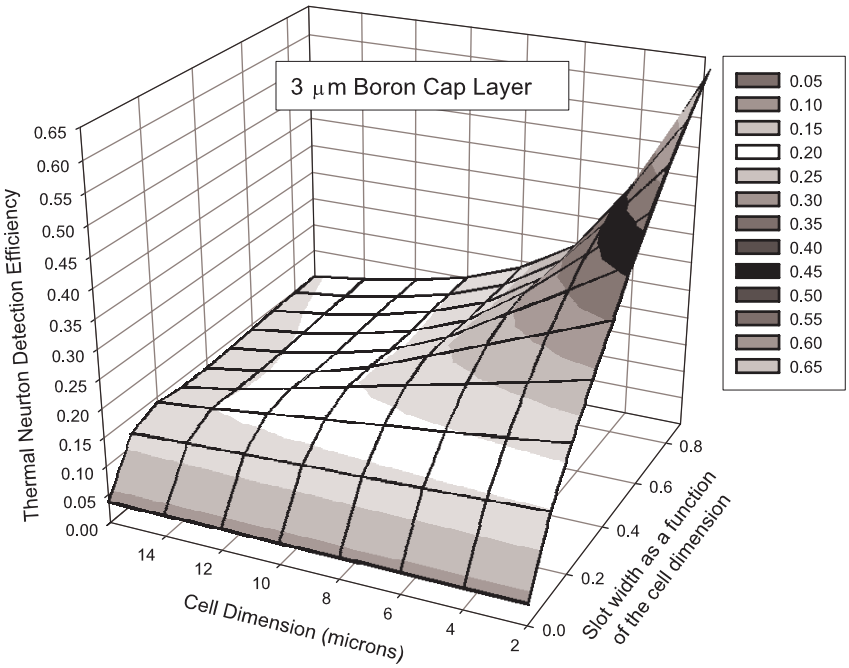

Figure 32. Detector efficiency for 50 μm deep channels filled with ^{10}B and with a 3 μm ^{10}B cap. Neutrons are normally incident on the surface opposite the cap.

7 Semiconductor Detectors with Cap and Internal Cylindrical Regions

Another design for a high-efficiency semiconductor detector is to etch many cylindrical holes into a semiconductor and then fill the holes with a neutron reactive material. A cap of the same reactive material is placed over the holes. This semiconductor detector is illustrated in Fig. 33 for a square array of holes and the geometric parameters for a unit cell of this detector are defined in Fig. 34.

As in the semiconductor detector with cap and channels, there are 6 distinct straight-line ion trajectories that can lead to energy being deposited in the semiconductor (see Fig. 35). In a type 1 event, an ion born in the cap heads toward the silicon and away from the rod (hole). The second ion, emitted in the opposite direction, heads away from the silicon and, thus, can deposit no energy in the silicon. In a type 2 event, an ion born in the cap heads toward the silicon and the central rod. The second ion heads away from the silicon. In a type 3 event, an ion born in the cap first enters the rod below the cap before heading towards the silicon. The second ion contributes nothing. In a type 4 event, ions are born in the rod below the cap and only the downward ion heads towards the silicon. In a type 5 event, ions are born in the rod below the cap and both head towards the silicon. Both ions can thus deposit energy in the silicon. In a type 6 event, ions are born in the cap above the rod and, thus, only the downward ion can possibly reach the silicon. Examples of energy-deposition spectra are shown in Figs. 36 and 37.

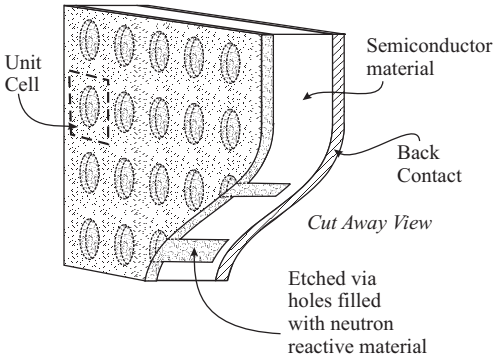

Figure 33. A semiconductor detector composed of a semiconductor into which a square array of cylindrical cavities have be etched filled with ^{10}B or ^{6}Li and a cap composed of the same converter is placed over the holes.

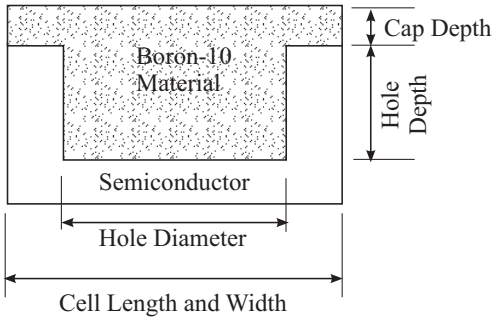

Figure 34. The geometric variables that define the unit cell of a semiconductor detectorwith a square array of cylindrical holes and a cap. The square cap has width X_{cap} and thickness T_{cap}. The hole depth is H_{rod} with radius R_{rod}.

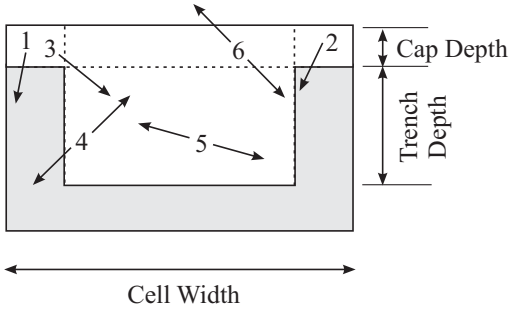

Figure 35. The six types of trajectories that can deposit energy in the silicon.

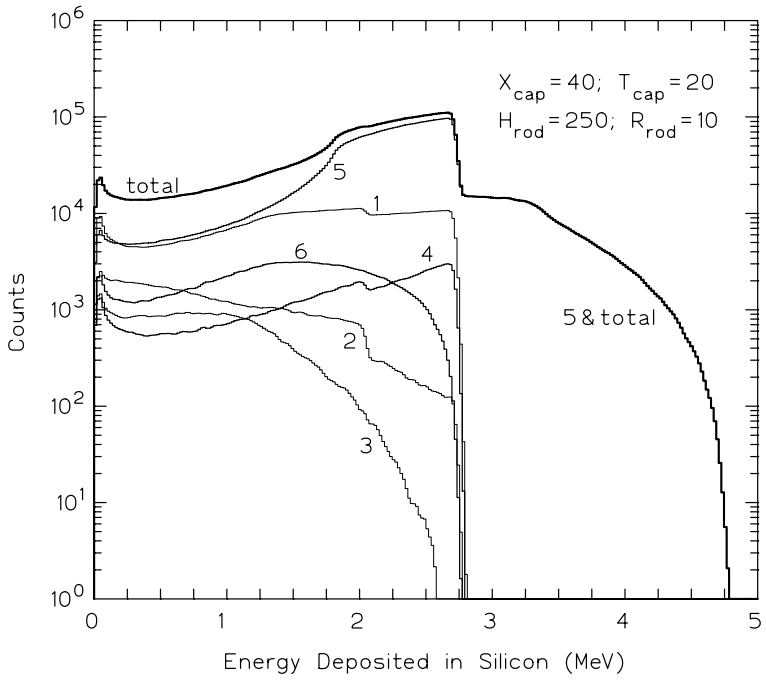

Figure 36. Calculated energy deposition spectrum (heavy line) for a semiconductor detector with cylindrical rods and cap of ^{6}LiF. Light lines show the various contributions made by the 6 possible trajectories. Neutrons are normally incident on the cap.

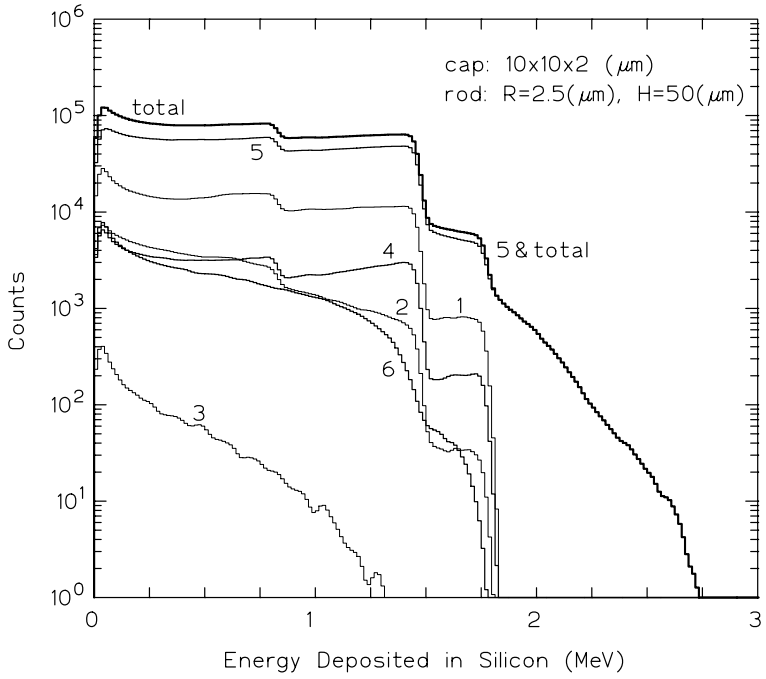

Figure 37. Calculated energy deposition spectrum (heavy line) for a semiconductor detector with cylindrical rods and cap of ^{10}B. Light lines show the various contributions made by the 6 possible ion trajectories. Neutrons are normally incident on the cap.

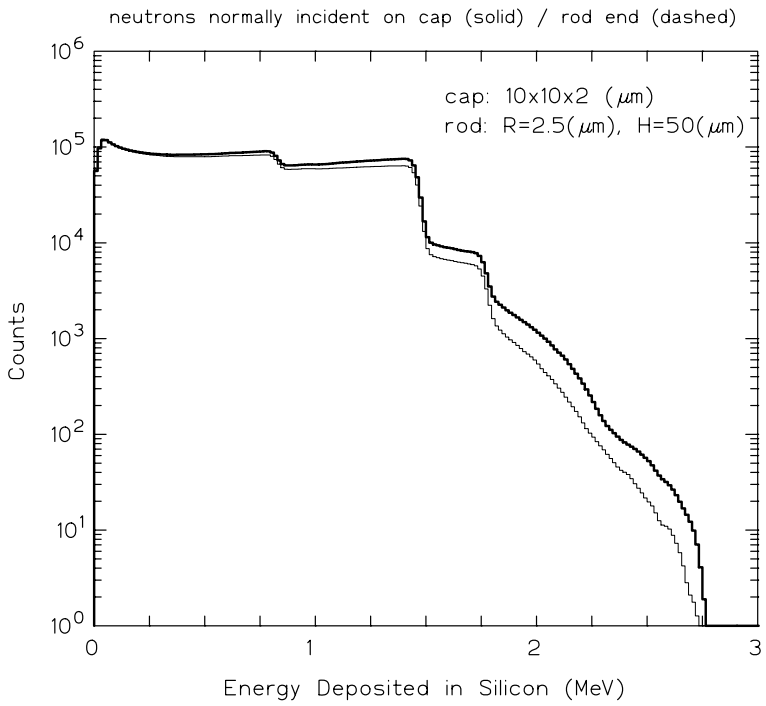

Figure 38. Energy deposition spectrum for a semiconductor detector with cylindrical rods and cap of ^{10}B. Light line is for neutrons normally incident on the cap and the dark line is for neutrons normally incident in the opposite direction.

As with the semiconductor detector with cap and channels, the semiconductor detector with cap and rods has a slightly higher efficiency when illuminated on the side opposite the cap than when the cap is normally illuminated. An example of this effect is shown in Fig. 38. For this example and with an energy cut-off of $E_{cut} = 300$ keV, the efficiencies were 13.8% and 15.4% for neutrons incident on the cap and the opposite side, respectively.

The reason for this directional dependence is that the cap acts absorbs ions produced in the portion of the rod adjacent to the cap. The greatest production rate of ions in the rod occurs in the region closest to the incident beam. When the bottom of the rod is the incident surface, one of the two ions produced near the end of the rod has a good chance of entering the silicon since any ion emitted in the direction of the beam will enter the silicon. By contrast, if the cap end of the channel is illuminated, ions produced in the top portion of the rod cannot reach silicon if they are emitted in the direction of the incoming neutrons.

7.1 Efficiency of a Semiconductor Detector with Cap and Rods

Extensive simulations were performed to estimate how the efficiency of a semiconductor detector with a cap and rods of neutron reactive material varies with the cell dimensions. Compilations of the results are presented in the Appendix in Tables A.5 to A.8. Some representative graphs constructed from data in the tables are shown in Figs. 39 and 40 for ^{6}LiF as the converter and in Figs. 41 to 52 for ^{10}B as the converter. For all these calculations, a discriminator level for the cut-off energy was taken as 300 keV.

For a unit cell with a cap of thickness T_{cap} and central hole of diameter D_{rod}, the stopping fraction is

$$P_{(n,x)} = [1 - \exp(-\Sigma_c T_{cap})] + \frac{1}{4}\pi \left(\frac{D_{rod}}{W_{cell}}\right)^2 [1 - \exp(-\Sigma_c H_{rod})].$$

Generally, the smaller the width of the square unit cell and the greater the rod diameter, the greater is the detector efficiency. There is also an optimum cap thickness beyond which the detector efficiency decreases. Also illumination of the semiconductor detector on the opposite side of the cap generally increases the efficiency by a few percentage points.

For the results shown in Figs. 39 and 40 for ^{6}LiF, the stopping fraction for a cell with $D_{rod}/W_{cell} = 0.6$ and no cap is 0.251. From Table A.6, the maximum efficiency is 0.228 for a cap thickness of about 15 and cap incidence. For reverse incidence, the maximum efficiency from Table A.8 is 0.246 for a cap thickness of about 35 μm.

For ^{10}B as the neutron reactive material, the stopping fraction for a cell with no cap and a central rod 50 μm long is tabulated in Table 11 for various D_{rod}/W_{cell} values. Also presented are values from Table A.8 for the smallest cell considered in this study, namely $W_{cell} = 20\mu$m. As a cell size decreases, the detection efficiency should converge to the stopping fraction. The results presented in Table 11 validate the Monte Carlo estimates of the detector efficiencies.

Table 11. Comparison of stopping fractions and detector efficiencies ϵ for a small ^{10}B square cell 20 μm in size.

Value	D_{rod}/W_{cell}								
	0.1	0.2	0.3	0.4	0.5	0.6	0.7	0.8	0.9
$P_{(n,\alpha)}$	0.007	0.028	0.063	0.112	0.174	0.251	0.342	0.446	0.565
eff ϵ	0.007	0.028	0.065	0.115	0.179	0.256	0.347	0.451	0.567

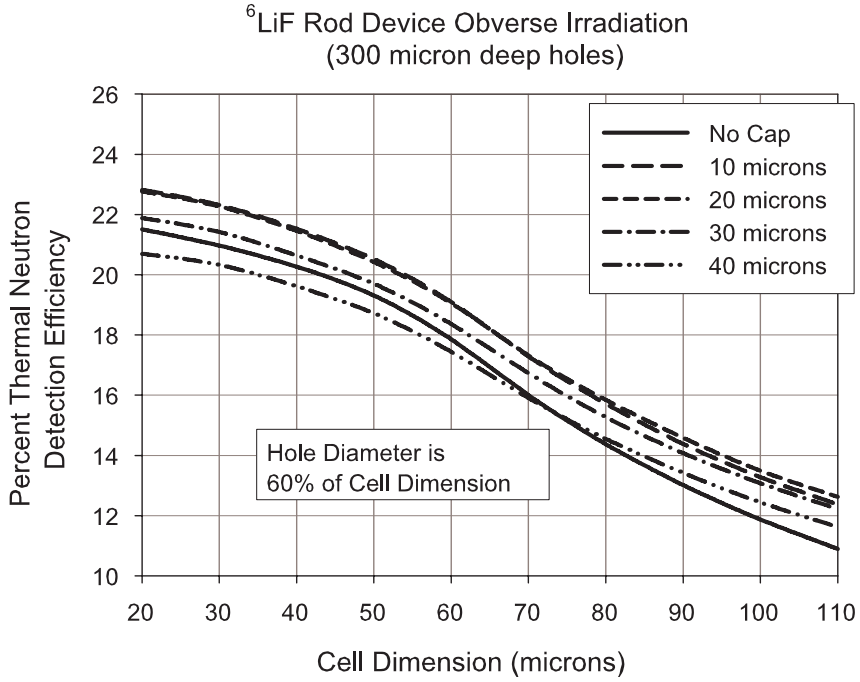

Figure 39. Detector efficiency for 300 μm deep holes filled with ^{6}LiF for various unit cell widths and thicknesses of the ^{6}LiF cap. The diameter of the hole is one-half of the unit cell width. Neutrons are normally incident on the cap

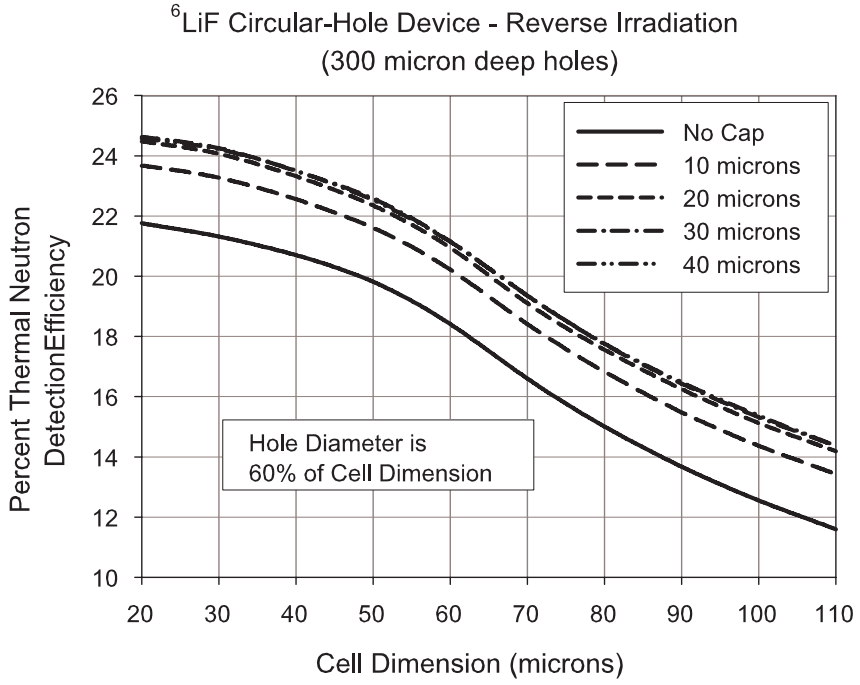

Figure 40. Detector efficiency for 300 μm deep holes filled with ^{6}LiF for various unit cell widths and thicknesses of the ^{6}LiF cap. The diameter of the hole is one-half of the unit cell width. Neutrons are normally incident on the surface opposite the cap.

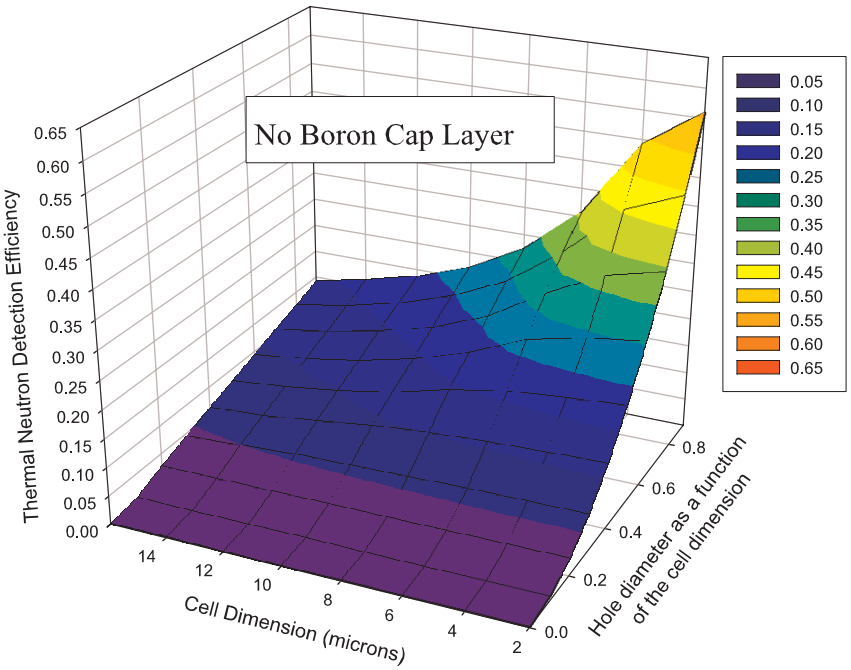

Figure 41. Detector efficiency for 50 μm deep holes filled with ^{10}B. Cap is not present. Neutrons are normally incident on the cap

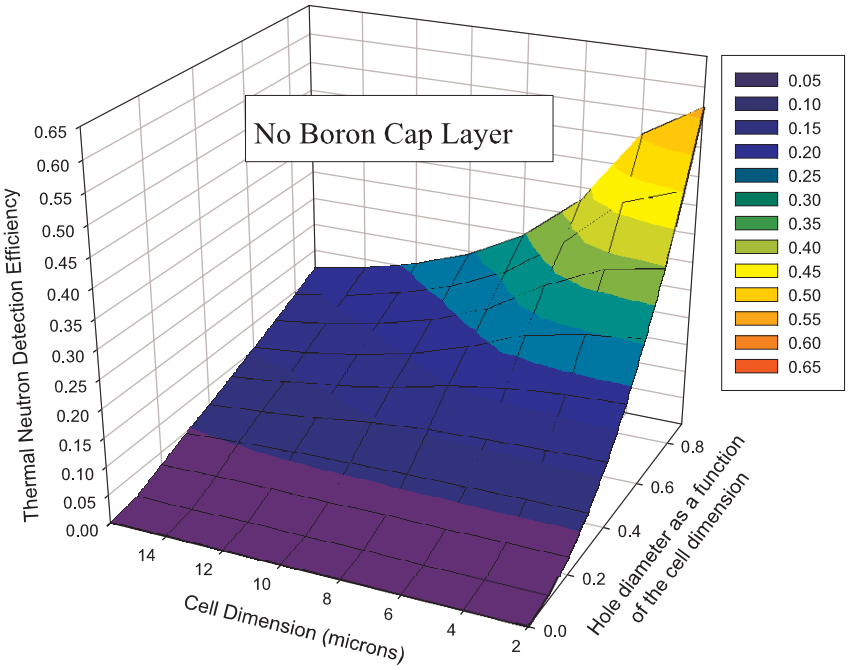

Figure 42. Detector efficiency for 50 μm deep holes filled with ^{10}B. Cap is not present. Neutrons are normally incident on the surface opposite the cap.

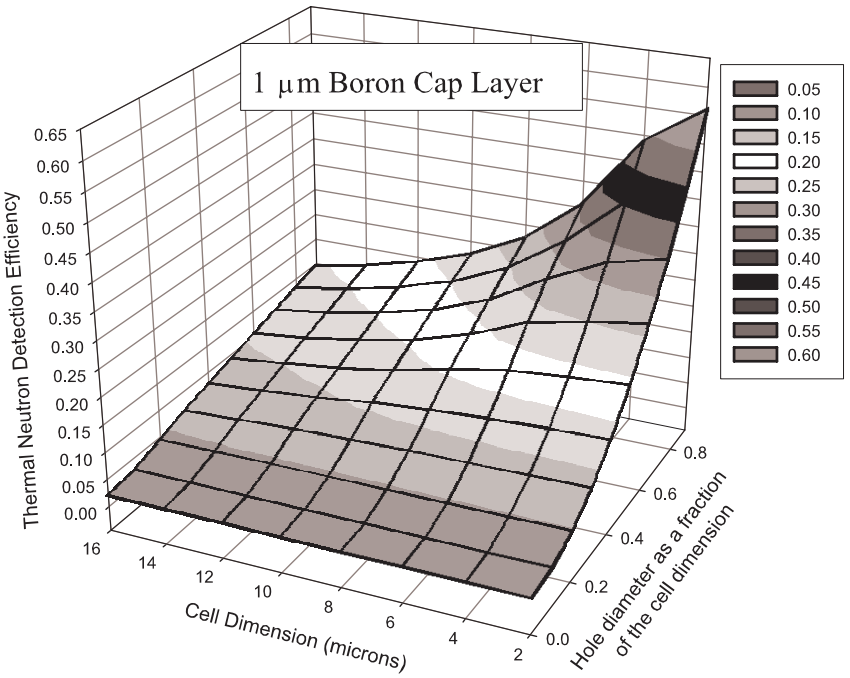

Figure 43. Detector efficiency for 50 μm deep holes filled with ^{10}B and with a 1 μm ^{10}B cap. Neutrons are normally incident on the cap

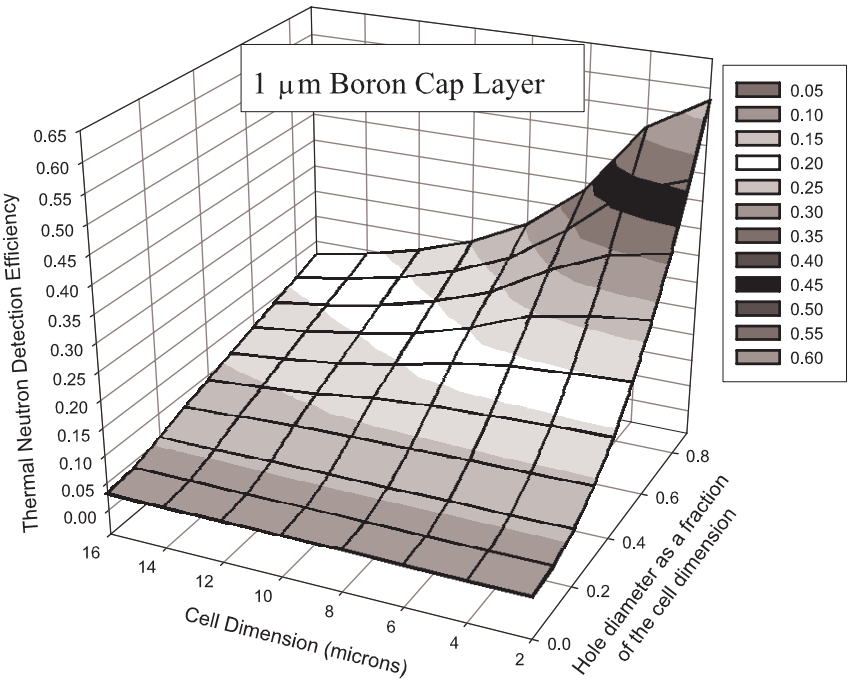

Figure 44. Detector efficiency for 50 μm deep holes filled with ^{10}B and with a 1 μm ^{10}B cap. Neutrons are normally incident on the surface opposite the cap.

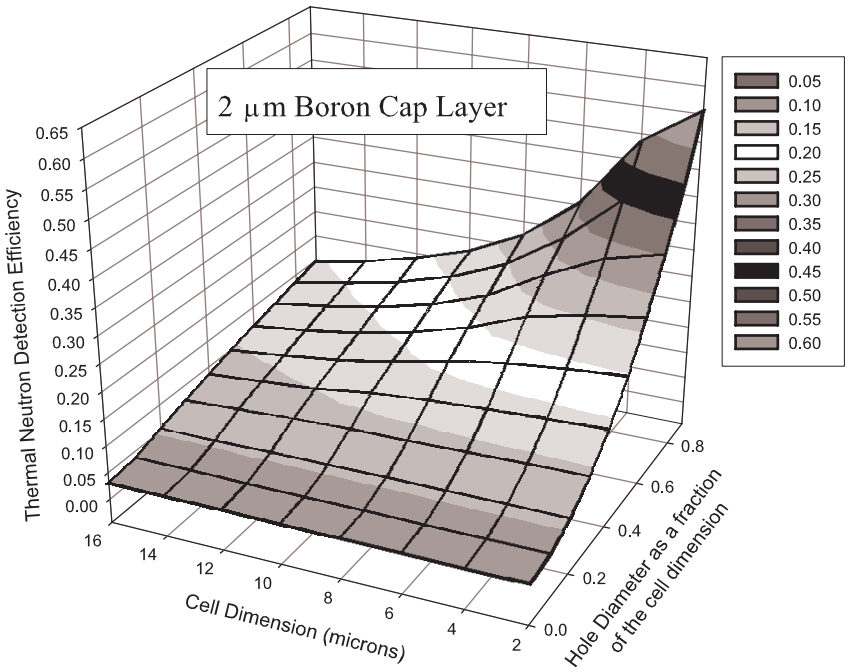

Figure 45. Detector efficiency for 50 μm deep holes filled with ^{10}B and with a 2 μm ^{10}B cap. Neutrons are normally incident on the cap

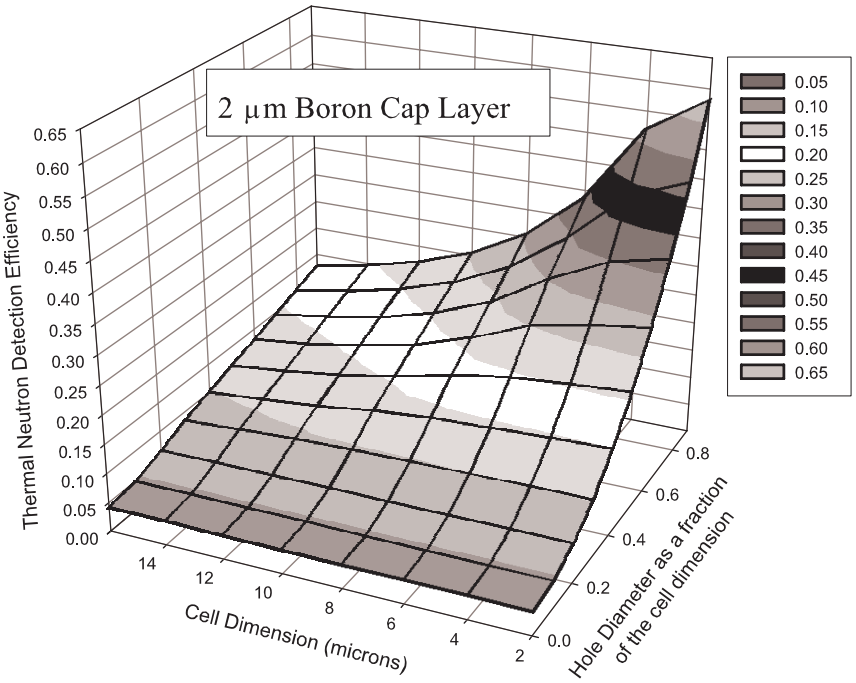

Figure 46. Detector efficiency for 50 μm deep holes filled with ^{10}B and with a 2 μm ^{10}B cap. Neutrons are normally incident on the surface opposite the cap.

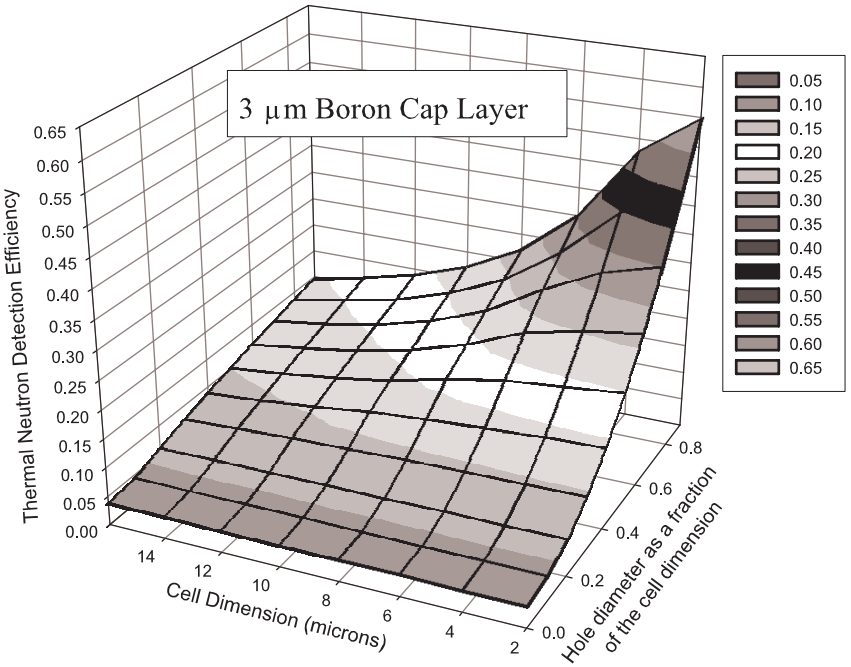

Figure 47. Detector efficiency for 50 μm deep holes filled with ^{10}B and with a 3 μm ^{10}B cap. Neutrons are normally incident on the cap

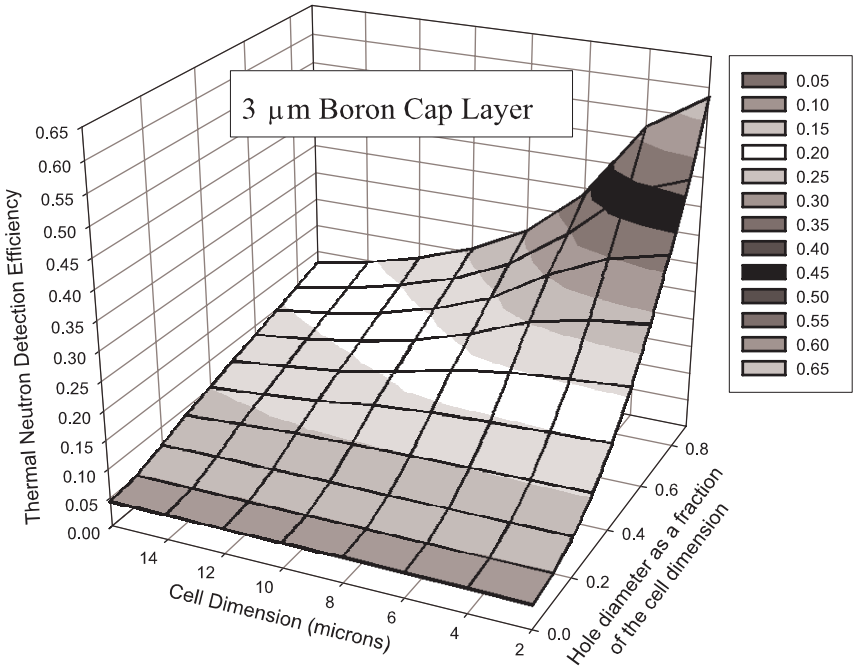

Figure 48. Detector efficiency for 50 μm deep holes filled with ^{10}B and with a 3 μm ^{10}B cap. Neutrons are normally incident on the surface opposite the cap.

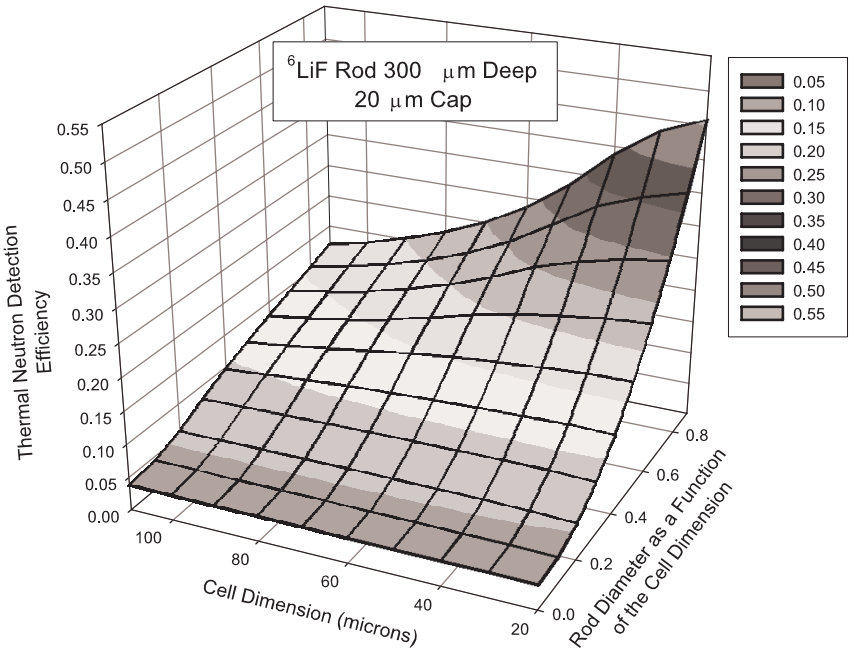

Figure 49. Detector efficiency for 300 μm deep holes filled with ^{6}LiF and with a 20 μm ^{6}LiF cap. Neutrons are normally incident on the cap

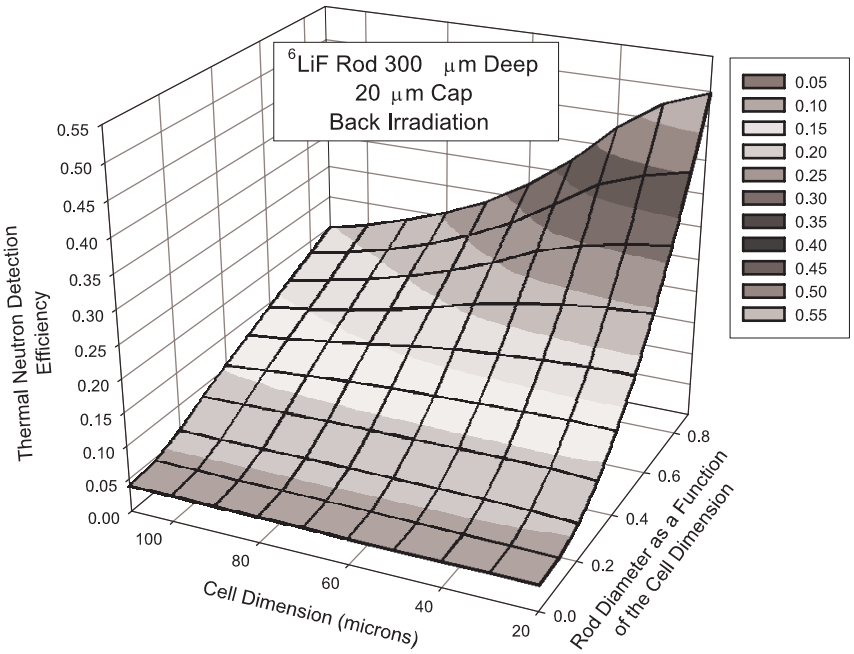

Figure 50. Detector efficiency for 50 μm holes filled with ^{6}LiF and with a 20 μm ^{6}LiF cap. Neutrons are normally incident on the surface opposite the cap.

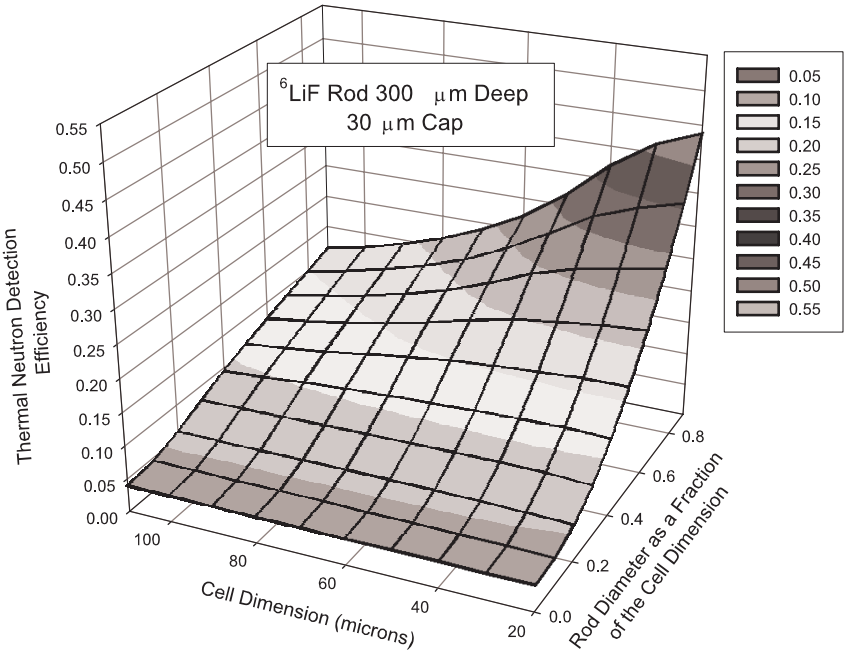

Figure 51. Detector efficiency for 300 μm deep holes filled with ^{6}LiF and with a 30 μm ^{6}LiF cap. Neutrons are normally incident on the cap

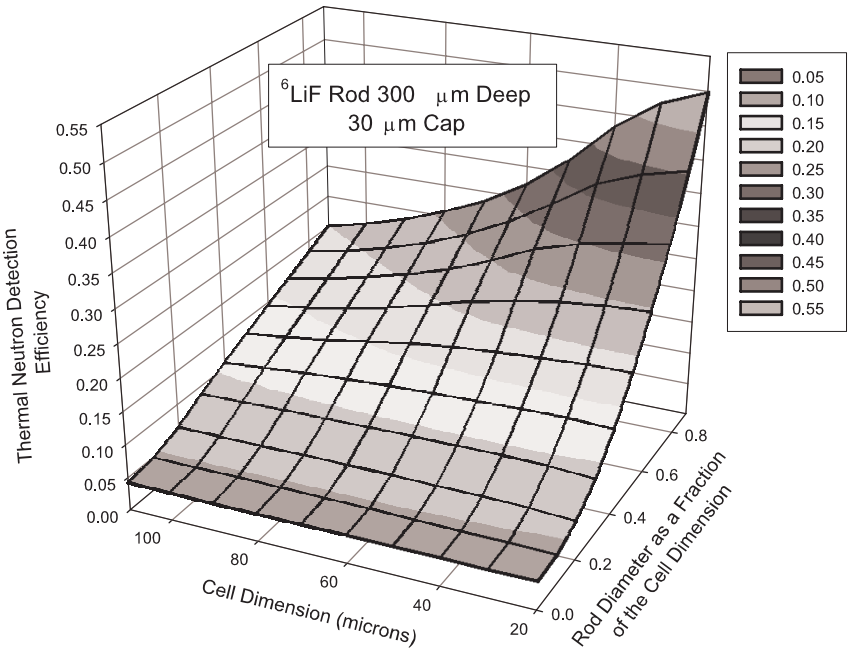

Figure 52. Detector efficiency for 50 μm holes filled with ^{6}LiF and with a 30 μm ^{6}LiF cap. Neutrons are normally incident on the surface opposite the cap.

8 Back-to-Back Channel Detectors with Caps

In Section 6, it is seen that semiconductor detectors with a cap and trenches of converter material could achieve relatively large detector efficiencies. With the presently available fabrication technology, it appears that such detectors can be made with efficiencies between 30 and 40%. However, such efficiencies can be doubled bay placing two channel detectors back-to-back with the silicon and converter regions overlapping (see Fig. 53).

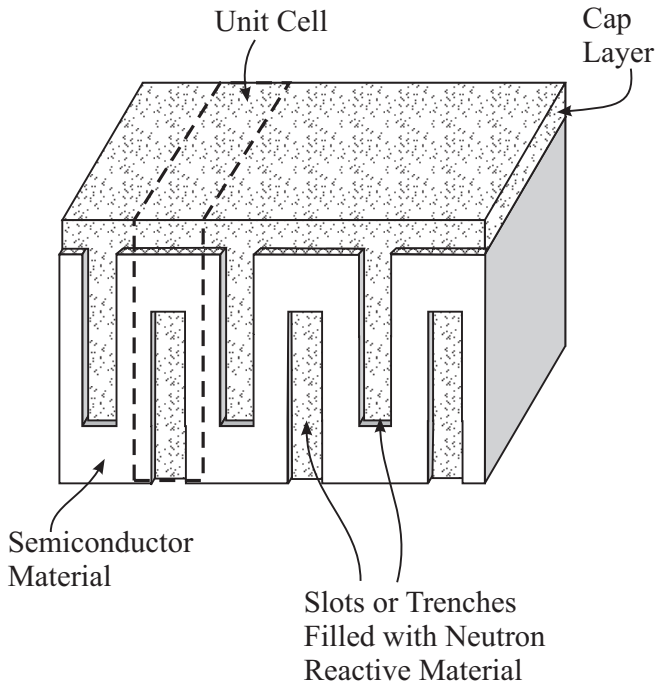

Figure 53. A back-to-back configuration of two semiconductor neutron detectors that doubles the efficiency of a single detector. Neutrons are normally incident on the top surface, and many of those that stream through the silicon in the top detector interact in the reactive material of the lower detector.

Details of the fabrication of two such sandwich detectors are shown in Figs. 54 and 55.

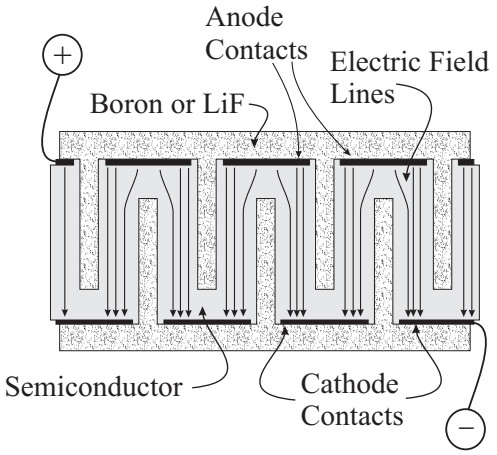

Figure 54. A sandwich semiconductor detector composed of a semiconductor into which a trenches of have be etched filled with ^{10}B or ^{6}Li and a cap composed of the same converter is placed over the trenches.

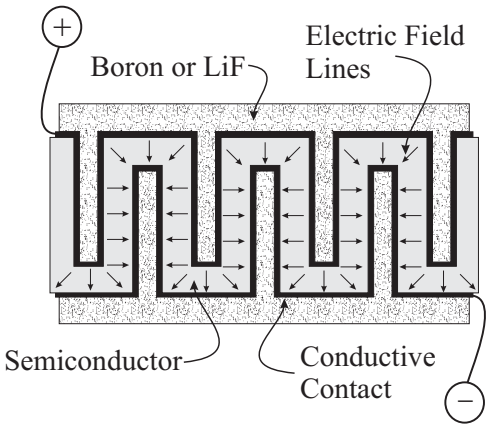

Figure 55. Another sandwich semiconductor detector composed of a semiconductor into which a trenches of have be etched filled with ^{10}B or ^{6}Li and a cap composed of the same converter is placed over the trenches.

BIBLIOGRAPHY

Jandel Scientific, "TableCurve," San Mataso, CA, 1996.

McGregor, D.S., M.D. Hammikg, Y.-H. Yang, H.K. Gersch, and R.T. Klann, "Design Consideration for Thin Film Coated Semiconductor Thermal Neutron Detectors—I: Basics Regarding Alpha Particle Emitting Neutron Reactive Films," *Nucl. Instr. Meth. A*, **500**, 272-308 (2003).

McGegor, D.S. and J.K. Shultis, "Spectrl Identification of Thin-Film-Coated and Solid-Form Semiconductor Neutron Detectors,", *Nucl. Instr. Meth. A*, **517**, 180–188 (2004).

Shultis, J.K., "Computation and Inversion of Ion Spectra for Neutron Depth Profiling of Curved Surfaces," *Nucl. Instr. Meth. A*, in press, 2004.

Shultis, J.K., "Notes on Neutron Depth Profiling," Engineering Experiment Station Report 298, Kansas State University, Manhattan, KS, Dec. 2003.

Ziegler, J.F. and J.P. Biersack, SRIM-2000.40, "Stopping and Range of Ions in Matter," 2002; available at `http://www.srim.org`

APPENDIX

Table A.1. Thermal-neutron detector efficiencies for a rectangular silicon cell of width W_{cell} and infinite in length and depth. A ^{6}LiF film of thickness T_{cap} coats one end. A 300-μm deep channel of width T_w is filled with ^{6}LiF. Neutrons are incident normally and incident on the cap, and detector cutoff energy $E_{cut} = 300$ keV.

T_w/W_{cell}	Cell Width X_{cap} (μm)									
	20	30	40	50	60	70	80	90	100	110
	Cap thickness $T_{cap} = 0$ μm									
0.0	0.0000	0.0000	0.0000	0.0000	0.0000	0.0000	0.0000	0.0000	0.0000	0.0000
0.1	0.0758	0.0745	0.0732	0.0719	0.0707	0.0694	0.0682	0.0671	0.0659	0.0647
0.2	0.1464	0.1414	0.1365	0.1317	0.1270	0.1224	0.1178	0.1133	0.1088	0.1044
0.3	0.2119	0.2012	0.1907	0.1802	0.1701	0.1599	0.1498	0.1398	0.1296	0.1195
0.4	0.2730	0.2546	0.2357	0.2177	0.1998	0.1818	0.1643	0.1463	0.1321	0.1206
0.5	0.3294	0.3003	0.2718	0.2439	0.2165	0.1885	0.1651	0.1477	0.1329	0.1217
0.6	0.3809	0.3399	0.2997	0.2595	0.2199	0.1889	0.1660	0.1486	0.1341	0.1225
0.7	0.4283	0.3727	0.3182	0.2637	0.2207	0.1903	0.1673	0.1493	0.1352	0.1234
0.8	0.4716	0.3996	0.3282	0.2646	0.2217	0.1911	0.1683	0.1501	0.1358	0.1244
0.9	0.5099	0.4191	0.3294	0.2651	0.2223	0.1918	0.1690	0.1511	0.1368	0.1252
	Cap thickness $T_{cap} = 10$ μm									
0.0	0.0263	0.0263	0.0262	0.0262	0.0263	0.0262	0.0263	0.0263	0.0263	0.0262
0.1	0.0977	0.0963	0.0949	0.0936	0.0923	0.0911	0.0899	0.0887	0.0874	0.0864
0.2	0.1637	0.1587	0.1535	0.1488	0.1440	0.1393	0.1347	0.1303	0.1259	0.1214
0.3	0.2250	0.2139	0.2030	0.1924	0.1823	0.1722	0.1624	0.1526	0.1430	0.1333
0.4	0.2812	0.2621	0.2438	0.2254	0.2079	0.1904	0.1731	0.1564	0.1427	0.1314
0.5	0.3335	0.3042	0.2759	0.2479	0.2209	0.1943	0.1719	0.1545	0.1409	0.1295
0.6	0.3814	0.3399	0.2993	0.2602	0.2219	0.1920	0.1699	0.1531	0.1391	0.1280
0.7	0.4248	0.3697	0.3149	0.2618	0.2200	0.1911	0.1689	0.1513	0.1375	0.1263
0.8	0.4636	0.3923	0.3227	0.2610	0.2190	0.1893	0.1673	0.1501	0.1363	0.1247
0.9	0.4993	0.4096	0.3217	0.2593	0.2184	0.1880	0.1664	0.1484	0.1356	0.1237
	Cap thickness $T_{cap} = 20$ μm									
0.0	0.0370	0.0371	0.0370	0.0369	0.0370	0.0370	0.0370	0.0371	0.0370	0.0370
0.1	0.1045	0.1031	0.1018	0.1004	0.0990	0.0975	0.0965	0.0952	0.0942	0.0929
0.2	0.1669	0.1615	0.1563	0.1516	0.1466	0.1424	0.1379	0.1336	0.1293	0.1253
0.3	0.2242	0.2133	0.2024	0.1921	0.1818	0.1724	0.1630	0.1533	0.1445	0.1351
0.4	0.2779	0.2584	0.2399	0.2219	0.2050	0.1884	0.1721	0.1560	0.1431	0.1323
0.5	0.3261	0.2976	0.2695	0.2424	0.2167	0.1908	0.1697	0.1535	0.1401	0.1299
0.6	0.3714	0.3304	0.2916	0.2532	0.2163	0.1880	0.1670	0.1510	0.1373	0.1270
0.7	0.4119	0.3578	0.3052	0.2539	0.2143	0.1860	0.1642	0.1479	0.1347	0.1237
0.8	0.4487	0.3789	0.3112	0.2520	0.2119	0.1836	0.1623	0.1459	0.1325	0.1210
0.9	0.4817	0.3944	0.3098	0.2502	0.2104	0.1812	0.1603	0.1434	0.1300	0.1197
	Cap thickness $T_{cap} = 30$ μm									
0.0	0.0387	0.0387	0.0387	0.0388	0.0387	0.0388	0.0386	0.0388	0.0387	0.0387
0.1	0.1027	0.1012	0.0997	0.0984	0.0972	0.0963	0.0951	0.0937	0.0928	0.0916
0.2	0.1617	0.1566	0.1515	0.1465	0.1423	0.1381	0.1340	0.1297	0.1259	0.1216
0.3	0.2162	0.2052	0.1947	0.1849	0.1755	0.1665	0.1574	0.1486	0.1398	0.1310
0.4	0.2664	0.2474	0.2299	0.2129	0.1971	0.1812	0.1660	0.1506	0.1380	0.1279
0.5	0.3121	0.2849	0.2579	0.2325	0.2078	0.1830	0.1628	0.1477	0.1352	0.1249
0.6	0.3549	0.3157	0.2786	0.2419	0.2070	0.1801	0.1601	0.1445	0.1316	0.1220
0.7	0.3934	0.3418	0.2910	0.2429	0.2043	0.1775	0.1569	0.1417	0.1295	0.1190
0.8	0.4283	0.3609	0.2968	0.2402	0.2023	0.1751	0.1551	0.1395	0.1268	0.1162
0.9	0.4591	0.3761	0.2957	0.2385	0.2003	0.1731	0.1526	0.1370	0.1244	0.1138
	Cap thickness $T_{cap} = 40$ μm									
0.0	0.0369	0.0368	0.0367	0.0368	0.0368	0.0369	0.0368	0.0369	0.0369	0.0367
0.1	0.0976	0.0960	0.0949	0.0937	0.0924	0.0914	0.0902	0.0889	0.0883	0.0869
0.2	0.1536	0.1487	0.1440	0.1395	0.1352	0.1313	0.1270	0.1233	0.1197	0.1158
0.3	0.2052	0.1950	0.1849	0.1759	0.1664	0.1582	0.1496	0.1415	0.1326	0.1243
0.4	0.2530	0.2357	0.2186	0.2028	0.1874	0.1723	0.1578	0.1432	0.1313	0.1216
0.5	0.2968	0.2703	0.2453	0.2203	0.1975	0.1739	0.1550	0.1400	0.1283	0.1189
0.6	0.3373	0.2999	0.2648	0.2301	0.1971	0.1711	0.1522	0.1369	0.1252	0.1160
0.7	0.3735	0.3243	0.2767	0.2307	0.1943	0.1689	0.1497	0.1344	0.1224	0.1134
0.8	0.4068	0.3429	0.2820	0.2284	0.1923	0.1665	0.1474	0.1322	0.1201	0.1108
0.9	0.4371	0.3570	0.2807	0.2270	0.1906	0.1648	0.1451	0.1302	0.1185	0.1084
	Cap thickness $T_{cap} = 50$ μm									
0.0	0.0351	0.0351	0.0349	0.0349	0.0349	0.0350	0.0350	0.0350	0.0348	0.0350
0.1	0.0927	0.0916	0.0904	0.0889	0.0877	0.0867	0.0858	0.0847	0.0841	0.0824
0.2	0.1460	0.1411	0.1366	0.1323	0.1283	0.1246	0.1208	0.1173	0.1135	0.1101
0.3	0.1952	0.1852	0.1757	0.1669	0.1587	0.1503	0.1422	0.1342	0.1264	0.1185
0.4	0.2404	0.2241	0.2081	0.1930	0.1782	0.1642	0.1499	0.1360	0.1243	0.1152
0.5	0.2823	0.2570	0.2331	0.2095	0.1878	0.1653	0.1471	0.1334	0.1223	0.1130
0.6	0.3200	0.2854	0.2511	0.2189	0.1866	0.1629	0.1449	0.1306	0.1192	0.1104
0.7	0.3557	0.3072	0.2632	0.2189	0.1848	0.1607	0.1425	0.1283	0.1166	0.1076
0.8	0.3857	0.3262	0.2676	0.2167	0.1825	0.1576	0.1400	0.1254	0.1141	0.1048
0.9	0.4147	0.3397	0.2671	0.2152	0.1808	0.1563	0.1384	0.1245	0.1118	0.1031

Table A.2. Thermal-neutron detector efficiencies for a rectangular silicon cell of width W_{cell} and infinite in length and depth. A ^{6}LiF film of thickness T_{cap} coats one end. A 300-μm deep channel of width T_w is filled with ^{6}LiF. Neutrons are incident normally and incident on the side opposite the cap, and detector cutoff energy $E_{cut} = 300$ keV.

T_w/W_{cell}	Cell Width X_{cap} (μm)									
	20	30	40	50	60	70	80	90	100	110
	Cap thickness $T_{cap} = 0$ μm									
0.0	0.0000	0.0000	0.0000	0.0000	0.0000	0.0000	0.0000	0.0000	0.0000	0.0000
0.1	0.0762	0.0750	0.0739	0.0728	0.0717	0.0706	0.0695	0.0684	0.0674	0.0663
0.2	0.1479	0.1434	0.1390	0.1346	0.1303	0.1259	0.1216	0.1173	0.1129	0.1087
0.3	0.2149	0.2053	0.1956	0.1857	0.1761	0.1661	0.1565	0.1468	0.1367	0.1270
0.4	0.2779	0.2606	0.2432	0.2260	0.2087	0.1912	0.1741	0.1565	0.1425	0.1313
0.5	0.3367	0.3096	0.2821	0.2553	0.2286	0.2011	0.1782	0.1610	0.1466	0.1356
0.6	0.3906	0.3517	0.3130	0.2742	0.2350	0.2047	0.1821	0.1649	0.1511	0.1393
0.7	0.4406	0.3877	0.3347	0.2815	0.2390	0.2094	0.1866	0.1688	0.1551	0.1435
0.8	0.4865	0.4174	0.3478	0.2855	0.2431	0.2130	0.1908	0.1728	0.1588	0.1479
0.9	0.5278	0.4401	0.3525	0.2894	0.2469	0.2168	0.1946	0.1773	0.1629	0.1515
	Cap thickness $T_{cap} = 10$ μm									
0.0	0.0265	0.0266	0.0265	0.0265	0.0265	0.0265	0.0265	0.0266	0.0265	0.0265
0.1	0.1001	0.0991	0.0978	0.0967	0.0956	0.0944	0.0933	0.0920	0.0909	0.0900
0.2	0.1693	0.1648	0.1602	0.1557	0.1510	0.1465	0.1422	0.1379	0.1336	0.1291
0.3	0.2341	0.2237	0.2134	0.2034	0.1935	0.1837	0.1739	0.1642	0.1547	0.1449
0.4	0.2940	0.2760	0.2584	0.2404	0.2230	0.2057	0.1885	0.1715	0.1576	0.1462
0.5	0.3501	0.3223	0.2947	0.2669	0.2400	0.2133	0.1902	0.1726	0.1588	0.1473
0.6	0.4020	0.3620	0.3221	0.2830	0.2445	0.2140	0.1917	0.1746	0.1603	0.1492
0.7	0.4495	0.3962	0.3413	0.2881	0.2459	0.2161	0.1936	0.1762	0.1619	0.1505
0.8	0.4925	0.4227	0.3532	0.2904	0.2477	0.2177	0.1954	0.1776	0.1639	0.1523
0.9	0.5322	0.4441	0.3553	0.2920	0.2503	0.2194	0.1978	0.1794	0.1664	0.1540
	Cap thickness $T_{cap} = 20$ μm									
0.0	0.0381	0.0380	0.0382	0.0380	0.0381	0.0381	0.0381	0.0381	0.0380	0.0380
0.1	0.1106	0.1093	0.1081	0.1068	0.1055	0.1042	0.1032	0.1020	0.1010	0.0998
0.2	0.1785	0.1735	0.1686	0.1640	0.1591	0.1550	0.1505	0.1460	0.1420	0.1377
0.3	0.2416	0.2311	0.2205	0.2103	0.2002	0.1905	0.1809	0.1710	0.1618	0.1521
0.4	0.3013	0.2822	0.2640	0.2458	0.2284	0.2116	0.1947	0.1774	0.1638	0.1522
0.5	0.3557	0.3273	0.2991	0.2714	0.2448	0.2176	0.1952	0.1779	0.1638	0.1529
0.6	0.4069	0.3661	0.3264	0.2864	0.2477	0.2180	0.1955	0.1787	0.1640	0.1531
0.7	0.4529	0.3987	0.3447	0.2910	0.2491	0.2188	0.1960	0.1788	0.1646	0.1529
0.8	0.4954	0.4249	0.3547	0.2924	0.2498	0.2199	0.1971	0.1802	0.1654	0.1539
0.9	0.5346	0.4452	0.3567	0.2939	0.2509	0.2207	0.1982	0.1804	0.1662	0.1555
	Cap thickness $T_{cap} = 30$ μm									
0.0	0.0414	0.0413	0.0413	0.0414	0.0414	0.0414	0.0413	0.0412	0.0414	0.0414
0.1	0.1134	0.1121	0.1106	0.1093	0.1084	0.1070	0.1060	0.1047	0.1037	0.1026
0.2	0.1809	0.1758	0.1709	0.1659	0.1616	0.1573	0.1529	0.1483	0.1444	0.1400
0.3	0.2438	0.2330	0.2223	0.2123	0.2022	0.1927	0.1829	0.1735	0.1639	0.1541
0.4	0.3028	0.2837	0.2654	0.2476	0.2302	0.2132	0.1963	0.1792	0.1652	0.1541
0.5	0.3570	0.3284	0.2997	0.2730	0.2458	0.2189	0.1965	0.1792	0.1657	0.1540
0.6	0.4077	0.3671	0.3270	0.2873	0.2490	0.2190	0.1965	0.1791	0.1653	0.1544
0.7	0.4541	0.3996	0.3452	0.2918	0.2495	0.2194	0.1964	0.1796	0.1659	0.1542
0.8	0.4962	0.4248	0.3553	0.2926	0.2501	0.2200	0.1981	0.1803	0.1663	0.1545
0.9	0.5350	0.4458	0.3573	0.2932	0.2512	0.2212	0.1985	0.1809	0.1666	0.1553
	Cap thickness $T_{cap} = 40$ μm									
0.0	0.0414	0.0415	0.0415	0.0414	0.0413	0.0412	0.0413	0.0413	0.0414	0.0411
0.1	0.1134	0.1119	0.1107	0.1094	0.1082	0.1071	0.1061	0.1047	0.1040	0.1026
0.2	0.1806	0.1758	0.1709	0.1661	0.1615	0.1573	0.1526	0.1486	0.1444	0.1399
0.3	0.2438	0.2329	0.2226	0.2124	0.2020	0.1929	0.1831	0.1733	0.1638	0.1541
0.4	0.3029	0.2840	0.2659	0.2480	0.2302	0.2132	0.1965	0.1795	0.1653	0.1540
0.5	0.3573	0.3285	0.3002	0.2726	0.2463	0.2187	0.1965	0.1797	0.1655	0.1540
0.6	0.4075	0.3670	0.3274	0.2876	0.2491	0.2188	0.1966	0.1788	0.1655	0.1542
0.7	0.4536	0.3989	0.3454	0.2917	0.2492	0.2195	0.1972	0.1795	0.1651	0.1546
0.8	0.4964	0.4252	0.3552	0.2925	0.2502	0.2202	0.1977	0.1801	0.1657	0.1546
0.9	0.5346	0.4454	0.3574	0.2941	0.2514	0.2217	0.1986	0.1810	0.1673	0.1552
	Cap thickness $T_{cap} = 50$ μm									
0.0	0.0413	0.0413	0.0413	0.0415	0.0416	0.0414	0.0414	0.0413	0.0413	0.0416
0.1	0.1136	0.1119	0.1110	0.1094	0.1080	0.1070	0.1059	0.1049	0.1037	0.1024
0.2	0.1807	0.1760	0.1711	0.1659	0.1615	0.1572	0.1529	0.1487	0.1444	0.1399
0.3	0.2438	0.2330	0.2223	0.2120	0.2024	0.1926	0.1830	0.1736	0.1640	0.1543
0.4	0.3029	0.2840	0.2656	0.2478	0.2305	0.2135	0.1964	0.1790	0.1655	0.1537
0.5	0.3571	0.3282	0.3003	0.2729	0.2461	0.2188	0.1962	0.1789	0.1657	0.1542
0.6	0.4074	0.3664	0.3268	0.2876	0.2490	0.2193	0.1966	0.1795	0.1656	0.1542
0.7	0.4545	0.3991	0.3452	0.2915	0.2493	0.2196	0.1973	0.1799	0.1655	0.1542
0.8	0.4961	0.4251	0.3549	0.2924	0.2501	0.2192	0.1972	0.1797	0.1661	0.1544
0.9	0.5345	0.4457	0.3574	0.2937	0.2513	0.2209	0.1986	0.1817	0.1665	0.1558

Table A.3. Thermal-neutron detector efficiencies for a rectangular silicon cell of width W_{cell} and infinite in length and depth. A ^{10}B film of thickness T_{cap} coats one end. A 50-μm deep channel of width T_w is filled with ^{10}B. Neutrons are incident normally and incident on the cap, and the detector cutoff energy E_{cut} is 300 keV.

T_w/W_{cell}	Cell Width X_{cap} (μm)							
	2	4	6	8	10	12	14	16
	Cap thickness $T_{cap} = 0$ μm							
0.0	0.0000	0.0000	0.0000	0.0000	0.0000	0.0000	0.0000	0.0000
0.1	0.0892	0.0867	0.0842	0.0817	0.0791	0.0767	0.0743	0.0720
0.2	0.1733	0.1630	0.1531	0.1437	0.1344	0.1252	0.1160	0.1070
0.3	0.2516	0.2292	0.2076	0.1871	0.1667	0.1465	0.1262	0.1135
0.4	0.3241	0.2851	0.2484	0.2123	0.1763	0.1509	0.1334	0.1209
0.5	0.3900	0.3316	0.2746	0.2191	0.1815	0.1575	0.1405	0.1279
0.6	0.4508	0.3666	0.2870	0.2228	0.1877	0.1637	0.1474	0.1348
0.7	0.5064	0.3922	0.2853	0.2272	0.1931	0.1696	0.1533	0.1413
0.8	0.5570	0.4075	0.2867	0.2290	0.1959	0.1734	0.1578	0.1459
0.9	0.6022	0.4133	0.2847	0.2273	0.1932	0.1717	0.1558	0.1456
	Cap thickness $T_{cap} = 1$ μm							
0.0	0.0298	0.0298	0.0298	0.0297	0.0297	0.0297	0.0298	0.0297
0.1	0.1253	0.1214	0.1174	0.1138	0.1100	0.1065	0.1030	0.0994
0.2	0.1988	0.1862	0.1742	0.1625	0.1514	0.1404	0.1295	0.1190
0.3	0.2670	0.2417	0.2171	0.1946	0.1720	0.1501	0.1282	0.1142
0.4	0.3301	0.2871	0.2478	0.2098	0.1720	0.1453	0.1276	0.1140
0.5	0.3882	0.3247	0.2654	0.2088	0.1697	0.1454	0.1282	0.1152
0.6	0.4411	0.3527	0.2719	0.2060	0.1698	0.1465	0.1295	0.1173
0.7	0.4906	0.3723	0.2644	0.2059	0.1705	0.1469	0.1307	0.1188
0.8	0.5345	0.3853	0.2637	0.2044	0.1697	0.1477	0.1318	0.1197
0.9	0.5749	0.3888	0.2614	0.2029	0.1688	0.1463	0.1303	0.1179
	Cap thickness $T_{cap} = 1.5$ μm							
0.0	0.0357	0.0356	0.0357	0.0356	0.0357	0.0356	0.0356	0.0357
0.1	0.1409	0.1365	0.1321	0.1277	0.1235	0.1195	0.1155	0.1115
0.2	0.2101	0.1964	0.1834	0.1711	0.1592	0.1474	0.1356	0.1245
0.3	0.2740	0.2474	0.2223	0.1984	0.1750	0.1521	0.1298	0.1151
0.4	0.3331	0.2895	0.2491	0.2102	0.1715	0.1442	0.1260	0.1122
0.5	0.3881	0.3231	0.2640	0.2063	0.1667	0.1419	0.1247	0.1117
0.6	0.4380	0.3485	0.2667	0.2008	0.1648	0.1417	0.1245	0.1118
0.7	0.4834	0.3666	0.2585	0.1996	0.1642	0.1412	0.1248	0.1127
0.8	0.5245	0.3757	0.2553	0.1969	0.1634	0.1405	0.1238	0.1121
0.9	0.5616	0.3777	0.2529	0.1964	0.1613	0.1384	0.1235	0.1108
	Cap thickness $T_{cap} = 2$ μm							
0.0	0.0391	0.0390	0.0391	0.0390	0.0391	0.0390	0.0391	0.0391
0.1	0.1553	0.1503	0.1454	0.1404	0.1360	0.1313	0.1267	0.1223
0.2	0.2201	0.2057	0.1920	0.1791	0.1664	0.1539	0.1414	0.1294
0.3	0.2800	0.2526	0.2267	0.2021	0.1780	0.1545	0.1313	0.1161
0.4	0.3357	0.2911	0.2497	0.2104	0.1714	0.1437	0.1250	0.1110
0.5	0.3864	0.3215	0.2614	0.2037	0.1643	0.1397	0.1220	0.1092
0.6	0.4335	0.3447	0.2625	0.1976	0.1612	0.1377	0.1212	0.1087
0.7	0.4764	0.3601	0.2528	0.1936	0.1588	0.1367	0.1202	0.1077
0.8	0.5145	0.3683	0.2490	0.1911	0.1572	0.1350	0.1189	0.1068
0.9	0.5487	0.3688	0.2457	0.1897	0.1554	0.1330	0.1170	0.1052
	Cap thickness $T_{cap} = 2.5$ μm							
0.0	0.0402	0.0402	0.0402	0.0400	0.0401	0.0401	0.0401	0.0401
0.1	0.1682	0.1627	0.1573	0.1520	0.1469	0.1420	0.1371	0.1322
0.2	0.2289	0.2136	0.1993	0.1857	0.1724	0.1594	0.1463	0.1338
0.3	0.2852	0.2565	0.2303	0.2050	0.1802	0.1558	0.1327	0.1171
0.4	0.3370	0.2921	0.2503	0.2103	0.1715	0.1427	0.1236	0.1099
0.5	0.3845	0.3195	0.2595	0.2016	0.1623	0.1377	0.1201	0.1069
0.6	0.4282	0.3398	0.2582	0.1932	0.1575	0.1340	0.1172	0.1048
0.7	0.4683	0.3535	0.2475	0.1894	0.1548	0.1320	0.1158	0.1039
0.8	0.5043	0.3598	0.2426	0.1855	0.1521	0.1295	0.1141	0.1027
0.9	0.5364	0.3590	0.2390	0.1830	0.1499	0.1273	0.1120	0.1006
	Cap thickness $T_{cap} = 3$ μm							
0.0	0.0394	0.0394	0.0393	0.0394	0.0394	0.0393	0.0395	0.0395
0.1	0.1795	0.1736	0.1679	0.1623	0.1568	0.1515	0.1463	0.1410
0.2	0.2362	0.2207	0.2058	0.1916	0.1778	0.1645	0.1509	0.1376
0.3	0.2889	0.2603	0.2333	0.2077	0.1819	0.1574	0.1335	0.1176
0.4	0.3373	0.2919	0.2504	0.2099	0.1707	0.1418	0.1229	0.1092
0.5	0.3816	0.3178	0.2570	0.1996	0.1596	0.1348	0.1177	0.1045
0.6	0.4226	0.3356	0.2542	0.1894	0.1542	0.1311	0.1141	0.1019
0.7	0.4594	0.3469	0.2419	0.1842	0.1501	0.1283	0.1123	0.0999
0.8	0.4932	0.3521	0.2362	0.1807	0.1476	0.1256	0.1098	0.0982
0.9	0.5229	0.3497	0.2318	0.1773	0.1452	0.1236	0.1076	0.0965

Table A.4. Thermal-neutron detector efficiencies for a rectangular silicon cell of width W_{cell} and infinite in length and depth. A ^{10}B film of thickness T_{cap} coats one end. A 50-μm deep channel of width T_w is filled with ^{10}B. Neutrons are incident normally and incident on the side opposite the cap, and detector cutoff energy $E_{cut} = 300$ keV.

T_w/W_{cell}	Cell Width X_{cap} (μm)							
	2	4	6	8	10	12	14	16
	Cap thickness $T_{cap} = 0$ μm							
0.0	0.0000	0.0000	0.0000	0.0000	0.0000	0.0000	0.0000	0.0000
0.1	0.0896	0.0873	0.0851	0.0829	0.0806	0.0784	0.0763	0.0741
0.2	0.1745	0.1654	0.1565	0.1478	0.1391	0.1303	0.1216	0.1127
0.3	0.2543	0.2342	0.2143	0.1948	0.1752	0.1554	0.1355	0.1228
0.4	0.3290	0.2934	0.2588	0.2238	0.1884	0.1634	0.1461	0.1339
0.5	0.3973	0.3434	0.2888	0.2344	0.1971	0.1736	0.1568	0.1444
0.6	0.4609	0.3820	0.3048	0.2414	0.2070	0.1832	0.1673	0.1550
0.7	0.5197	0.4114	0.3069	0.2494	0.2159	0.1927	0.1768	0.1648
0.8	0.5736	0.4307	0.3117	0.2549	0.2222	0.2001	0.1847	0.1733
0.9	0.6221	0.4399	0.3134	0.2565	0.2232	0.2022	0.1864	0.1764
	Cap thickness $T_{cap} = 1$ μm							
0.0	0.0301	0.0301	0.0301	0.0301	0.0300	0.0300	0.0301	0.0300
0.1	0.1283	0.1250	0.1215	0.1183	0.1150	0.1118	0.1086	0.1054
0.2	0.2046	0.1938	0.1830	0.1721	0.1614	0.1508	0.1402	0.1296
0.3	0.2764	0.2539	0.2310	0.2091	0.1870	0.1648	0.1425	0.1283
0.4	0.3434	0.3043	0.2666	0.2290	0.1906	0.1633	0.1453	0.1313
0.5	0.4062	0.3467	0.2887	0.2315	0.1914	0.1668	0.1493	0.1360
0.6	0.4636	0.3800	0.2993	0.2321	0.1953	0.1714	0.1543	0.1413
0.7	0.5177	0.4038	0.2948	0.2351	0.1990	0.1754	0.1587	0.1467
0.8	0.5663	0.4211	0.2975	0.2370	0.2018	0.1796	0.1629	0.1510
0.9	0.6117	0.4281	0.2991	0.2388	0.2040	0.1808	0.1651	0.1519
	Cap thickness $T_{cap} = 1.5$ μm							
0.0	0.0364	0.0363	0.0364	0.0364	0.0363	0.0363	0.0363	0.0364
0.1	0.1469	0.1432	0.1392	0.1353	0.1315	0.1279	0.1242	0.1203
0.2	0.2202	0.2081	0.1963	0.1848	0.1733	0.1616	0.1501	0.1388
0.3	0.2887	0.2647	0.2411	0.2178	0.1943	0.1708	0.1474	0.1321
0.4	0.3533	0.3126	0.2734	0.2341	0.1943	0.1657	0.1469	0.1323
0.5	0.4135	0.3517	0.2932	0.2334	0.1924	0.1664	0.1489	0.1350
0.6	0.4692	0.3827	0.2999	0.2313	0.1939	0.1696	0.1517	0.1387
0.7	0.5200	0.4057	0.2945	0.2329	0.1968	0.1724	0.1554	0.1426
0.8	0.5668	0.4199	0.2945	0.2333	0.1987	0.1752	0.1578	0.1455
0.9	0.6096	0.4255	0.2952	0.2361	0.2000	0.1759	0.1603	0.1476
	Cap thickness $T_{cap} = 2$ μm							
0.0	0.0404	0.0403	0.0404	0.0404	0.0403	0.0404	0.0403	0.0404
0.1	0.1653	0.1608	0.1565	0.1521	0.1479	0.1436	0.1392	0.1350
0.2	0.2356	0.2227	0.2100	0.1976	0.1852	0.1726	0.1599	0.1473
0.3	0.3015	0.2762	0.2514	0.2267	0.2022	0.1773	0.1527	0.1365
0.4	0.3636	0.3213	0.2805	0.2399	0.1985	0.1692	0.1493	0.1345
0.5	0.4208	0.3580	0.2972	0.2366	0.1940	0.1679	0.1492	0.1356
0.6	0.4741	0.3871	0.3021	0.2324	0.1942	0.1690	0.1515	0.1382
0.7	0.5237	0.4078	0.2947	0.2315	0.1946	0.1713	0.1538	0.1400
0.8	0.5683	0.4204	0.2938	0.2324	0.1965	0.1730	0.1552	0.1426
0.9	0.6090	0.4245	0.2934	0.2341	0.1978	0.1735	0.1569	0.1442
	Cap thickness $T_{cap} = 2.5$ μm							
0.0	0.0422	0.0422	0.0421	0.0421	0.0422	0.0422	0.0422	0.0423
0.1	0.1831	0.1781	0.1733	0.1684	0.1637	0.1590	0.1542	0.1494
0.2	0.2505	0.2368	0.2233	0.2098	0.1965	0.1832	0.1698	0.1564
0.3	0.3140	0.2876	0.2615	0.2358	0.2099	0.1837	0.1582	0.1414
0.4	0.3734	0.3301	0.2878	0.2461	0.2037	0.1724	0.1516	0.1366
0.5	0.4285	0.3646	0.3021	0.2399	0.1965	0.1699	0.1505	0.1363
0.6	0.4797	0.3914	0.3049	0.2337	0.1947	0.1689	0.1509	0.1373
0.7	0.5273	0.4105	0.2959	0.2326	0.1946	0.1696	0.1524	0.1391
0.8	0.5704	0.4213	0.2937	0.2313	0.1949	0.1706	0.1537	0.1411
0.9	0.6095	0.4235	0.2926	0.2316	0.1958	0.1713	0.1546	0.1422
	Cap thickness $T_{cap} = 3$ μm							
0.0	0.0424	0.0425	0.0424	0.0425	0.0426	0.0424	0.0425	0.0425
0.1	0.2003	0.1949	0.1896	0.1843	0.1791	0.1738	0.1687	0.1634
0.2	0.2652	0.2507	0.2363	0.2219	0.2079	0.1938	0.1793	0.1649
0.3	0.3264	0.2989	0.2716	0.2448	0.2174	0.1904	0.1634	0.1458
0.4	0.3833	0.3387	0.2955	0.2517	0.2080	0.1759	0.1546	0.1391
0.5	0.4365	0.3715	0.3069	0.2433	0.1989	0.1711	0.1517	0.1369
0.6	0.4853	0.3960	0.3076	0.2353	0.1959	0.1697	0.1509	0.1371
0.7	0.5309	0.4132	0.2967	0.2327	0.1942	0.1698	0.1518	0.1379
0.8	0.5720	0.4225	0.2932	0.2315	0.1946	0.1697	0.1521	0.1390
0.9	0.6096	0.4237	0.2913	0.2306	0.1947	0.1704	0.1528	0.1401

Table A.5. Thermal-neutron detector efficiencies for a square silicon cell of width W_{cell} and infinite in depth. A ^{10}B film of thickness T_{cap} coats one end. A 50-μm deep hole in the center of the cell with diameter D is filled with ^{10}B. Neutrons are incident normally on the cap, and the detector cutoff energy E_{cut} is 300 keV.

D/W_{cell}	Cell Width X_{cap} (μm)							
	2	4	6	8	10	12	14	16
	Cap thickness $T_{cap} = 0$ μm							
0.0	0.0000	0.0000	0.0000	0.0000	0.0000	0.0000	0.0000	0.0000
0.1	0.0072	0.0072	0.0072	0.0071	0.0071	0.0071	0.0070	0.0070
0.2	0.0288	0.0286	0.0282	0.0278	0.0273	0.0268	0.0261	0.0253
0.3	0.0645	0.0636	0.0621	0.0602	0.0578	0.0545	0.0496	0.0440
0.4	0.1143	0.1113	0.1069	0.1010	0.0918	0.0783	0.0682	0.0605
0.5	0.1776	0.1708	0.1604	0.1435	0.1181	0.1001	0.0867	0.0765
0.6	0.2542	0.2407	0.2182	0.1760	0.1440	0.1218	0.1048	0.0929
0.7	0.3437	0.3193	0.2703	0.2091	0.1699	0.1434	0.1237	0.1084
0.8	0.4453	0.4041	0.3130	0.2414	0.1965	0.1648	0.1416	0.1248
0.9	0.5587	0.4910	0.3569	0.2740	0.2216	0.1859	0.1603	0.1408
	Cap thickness $T_{cap} = 1$ μm							
0.0	0.0298	0.0297	0.0298	0.0298	0.0298	0.0298	0.0297	0.0298
0.1	0.0365	0.0365	0.0365	0.0364	0.0364	0.0364	0.0363	0.0362
0.2	0.0568	0.0565	0.0560	0.0555	0.0550	0.0545	0.0537	0.0529
0.3	0.0904	0.0891	0.0873	0.0852	0.0828	0.0798	0.0750	0.0697
0.4	0.1371	0.1335	0.1285	0.1225	0.1138	0.1007	0.0912	0.0837
0.5	0.1965	0.1886	0.1777	0.1612	0.1367	0.1195	0.1068	0.0970
0.6	0.2686	0.2531	0.2302	0.1898	0.1590	0.1376	0.1217	0.1100
0.7	0.3526	0.3257	0.2770	0.2184	0.1806	0.1551	0.1361	0.1221
0.8	0.4482	0.4043	0.3151	0.2462	0.2025	0.1723	0.1506	0.1338
0.9	0.5550	0.4853	0.3538	0.2740	0.2233	0.1894	0.1643	0.1454
	Cap thickness $T_{cap} = 1.5$ μm							
0.0	0.0357	0.0356	0.0357	0.0356	0.0357	0.0357	0.0356	0.0356
0.1	0.0422	0.0422	0.0422	0.0420	0.0421	0.0420	0.0419	0.0418
0.2	0.0619	0.0617	0.0611	0.0606	0.0601	0.0594	0.0589	0.0580
0.3	0.0948	0.0932	0.0914	0.0893	0.0870	0.0839	0.0794	0.0740
0.4	0.1402	0.1362	0.1312	0.1253	0.1168	0.1038	0.0946	0.0874
0.5	0.1982	0.1895	0.1788	0.1625	0.1388	0.1218	0.1095	0.0998
0.6	0.2680	0.2522	0.2296	0.1897	0.1597	0.1387	0.1234	0.1117
0.7	0.3499	0.3227	0.2748	0.2174	0.1804	0.1554	0.1369	0.1229
0.8	0.4431	0.3987	0.3110	0.2439	0.2010	0.1708	0.1500	0.1344
0.9	0.5467	0.4771	0.3486	0.2698	0.2199	0.1870	0.1632	0.1441
	Cap thickness $T_{cap} = 2$ μm							
0.0	0.0390	0.0389	0.0390	0.0390	0.0391	0.0391	0.0390	0.0391
0.1	0.0454	0.0454	0.0454	0.0454	0.0452	0.0451	0.0452	0.0451
0.2	0.0648	0.0643	0.0637	0.0633	0.0626	0.0622	0.0615	0.0608
0.3	0.0967	0.0948	0.0930	0.0912	0.0889	0.0859	0.0812	0.0763
0.4	0.1408	0.1368	0.1318	0.1259	0.1174	0.1053	0.0960	0.0888
0.5	0.1972	0.1886	0.1775	0.1619	0.1382	0.1223	0.1101	0.1008
0.6	0.2655	0.2491	0.2268	0.1880	0.1589	0.1382	0.1234	0.1121
0.7	0.3450	0.3179	0.2707	0.2141	0.1787	0.1544	0.1364	0.1229
0.8	0.4357	0.3918	0.3060	0.2397	0.1981	0.1695	0.1485	0.1331
0.9	0.5370	0.4679	0.3423	0.2653	0.2171	0.1841	0.1602	0.1425
	Cap thickness $T_{cap} = 2.5$ μm							
0.0	0.0402	0.0401	0.0401	0.0401	0.0401	0.0400	0.0401	0.0401
0.1	0.0464	0.0463	0.0462	0.0462	0.0462	0.0461	0.0460	0.0460
0.2	0.0652	0.0647	0.0640	0.0638	0.0631	0.0626	0.0620	0.0612
0.3	0.0962	0.0944	0.0925	0.0908	0.0884	0.0855	0.0813	0.0761
0.4	0.1389	0.1350	0.1302	0.1245	0.1164	0.1044	0.0954	0.0883
0.5	0.1941	0.1857	0.1748	0.1595	0.1368	0.1208	0.1091	0.0999
0.6	0.2608	0.2446	0.2229	0.1851	0.1569	0.1364	0.1219	0.1107
0.7	0.3383	0.3110	0.2649	0.2100	0.1757	0.1513	0.1343	0.1210
0.8	0.4264	0.3831	0.2995	0.2354	0.1938	0.1661	0.1457	0.1308
0.9	0.5250	0.4568	0.3347	0.2594	0.2125	0.1801	0.1568	0.1395
	Cap thickness $T_{cap} = 3$ μm							
0.0	0.0394	0.0394	0.0394	0.0394	0.0394	0.0393	0.0395	0.0392
0.1	0.0456	0.0454	0.0454	0.0453	0.0453	0.0453	0.0452	0.0451
0.2	0.0639	0.0633	0.0626	0.0622	0.0618	0.0613	0.0606	0.0599
0.3	0.0940	0.0923	0.0905	0.0887	0.0864	0.0838	0.0796	0.0746
0.4	0.1361	0.1320	0.1271	0.1219	0.1138	0.1020	0.0932	0.0866
0.5	0.1898	0.1812	0.1707	0.1559	0.1335	0.1180	0.1064	0.0977
0.6	0.2546	0.2391	0.2175	0.1804	0.1526	0.1333	0.1194	0.1081
0.7	0.3299	0.3036	0.2587	0.2051	0.1710	0.1478	0.1311	0.1181
0.8	0.4160	0.3735	0.2925	0.2292	0.1893	0.1620	0.1423	0.1273
0.9	0.5122	0.4460	0.3270	0.2532	0.2072	0.1756	0.1534	0.1365

Table A.6. Thermal-neutron detector efficiencies for a square silicon cell of width W_{cell} and infinite in depth. A ^{10}B film of thickness T_{cap} coats one end. A 50-μm deep hole in the center of the cell with diameter D is filled with ^{10}B. Neutrons are incident normally and uniformly on the end opposite the cap. The detector cutoff energy E_{cut} is 300 keV.

D/W_{cell}	Cell Width X_{cap} (μm)							
	2	4	6	8	10	12	14	16
	Cap thickness $T_{cap} = 0$ μm							
0.0	0.0000	0.0000	0.0000	0.0000	0.0000	0.0000	0.0000	0.0000
0.1	0.0072	0.0072	0.0072	0.0072	0.0071	0.0071	0.0071	0.0070
0.2	0.0288	0.0287	0.0285	0.0282	0.0278	0.0273	0.0267	0.0260
0.3	0.0647	0.0640	0.0630	0.0614	0.0593	0.0563	0.0515	0.0461
0.4	0.1147	0.1127	0.1091	0.1039	0.0952	0.0820	0.0720	0.0644
0.5	0.1786	0.1737	0.1647	0.1488	0.1239	0.1062	0.0930	0.0830
0.6	0.2562	0.2457	0.2253	0.1843	0.1527	0.1309	0.1143	0.1026
0.7	0.3470	0.3270	0.2807	0.2207	0.1824	0.1562	0.1369	0.1218
0.8	0.4507	0.4157	0.3277	0.2572	0.2131	0.1820	0.1591	0.1424
0.9	0.5668	0.5070	0.3760	0.2947	0.2430	0.2079	0.1826	0.1637
	Cap thickness $T_{cap} = 1$ μm							
0.0	0.0301	0.0301	0.0301	0.0301	0.0301	0.0301	0.0301	0.0301
0.1	0.0370	0.0370	0.0369	0.0369	0.0369	0.0369	0.0368	0.0368
0.2	0.0577	0.0575	0.0572	0.0569	0.0565	0.0559	0.0555	0.0547
0.3	0.0921	0.0913	0.0900	0.0883	0.0864	0.0836	0.0788	0.0734
0.4	0.1402	0.1378	0.1338	0.1287	0.1203	0.1073	0.0974	0.0897
0.5	0.2018	0.1960	0.1868	0.1712	0.1462	0.1291	0.1160	0.1062
0.6	0.2766	0.2649	0.2444	0.2037	0.1725	0.1508	0.1348	0.1227
0.7	0.3646	0.3430	0.2965	0.2367	0.1990	0.1724	0.1534	0.1392
0.8	0.4648	0.4278	0.3397	0.2695	0.2250	0.1951	0.1722	0.1559
0.9	0.5774	0.5157	0.3850	0.3037	0.2519	0.2173	0.1923	0.1726
	Cap thickness $T_{cap} = 2$ μm							
0.0	0.0404	0.0403	0.0403	0.0404	0.0404	0.0403	0.0404	0.0403
0.1	0.0472	0.0471	0.0470	0.0470	0.0470	0.0470	0.0470	0.0469
0.2	0.0677	0.0672	0.0669	0.0666	0.0662	0.0657	0.0652	0.0645
0.3	0.1016	0.1005	0.0989	0.0974	0.0955	0.0926	0.0881	0.0827
0.4	0.1491	0.1461	0.1421	0.1371	0.1287	0.1157	0.1059	0.0984
0.5	0.2097	0.2034	0.1937	0.1785	0.1537	0.1366	0.1238	0.1139
0.6	0.2840	0.2709	0.2507	0.2101	0.1791	0.1575	0.1413	0.1291
0.7	0.3705	0.3478	0.3015	0.2419	0.2041	0.1778	0.1591	0.1445
0.8	0.4696	0.4318	0.3436	0.2737	0.2291	0.1986	0.1769	0.1605
0.9	0.5809	0.5195	0.3875	0.3062	0.2547	0.2194	0.1949	0.1758
	Cap thickness $T_{cap} = 3$ μm							
0.0	0.0424	0.0424	0.0424	0.0425	0.0425	0.0425	0.0424	0.0424
0.1	0.0493	0.0492	0.0492	0.0491	0.0491	0.0490	0.0490	0.0490
0.2	0.0697	0.0693	0.0689	0.0686	0.0681	0.0677	0.0673	0.0665
0.3	0.1038	0.1022	0.1008	0.0993	0.0972	0.0944	0.0900	0.0846
0.4	0.1509	0.1476	0.1438	0.1386	0.1305	0.1173	0.1078	0.1002
0.5	0.2113	0.2047	0.1954	0.1801	0.1555	0.1382	0.1252	0.1155
0.6	0.2853	0.2725	0.2517	0.2112	0.1806	0.1588	0.1432	0.1308
0.7	0.3715	0.3490	0.3023	0.2431	0.2055	0.1791	0.1605	0.1459
0.8	0.4708	0.4326	0.3447	0.2739	0.2298	0.2000	0.1774	0.1609
0.9	0.5817	0.5194	0.3883	0.3064	0.2559	0.2207	0.1952	0.1766

Table A.7. Thermal-neutron detector efficiencies for a square silicon cell of width W_{cell} and infinite in depth. A ^{6}LiF film of thickness T_{cap} coats one end. A 300-μm deep hole in the center of the cell with diameter D is filled with ^{6}LiF. Neutrons are incident normally and uniformly on the cap. The detector cutoff energy E_{cut} is 300 keV.

D/W_{cell}	Cell Width X_{cap} (μm)									
	20	30	40	50	60	70	80	90	100	110
	Cap thickness $T_{cap} = 0$ μm									
0.0	0.0000	0.0000	0.0000	0.0000	0.0000	0.0000	0.0000	0.0000	0.0000	0.0000
0.1	0.0061	0.0061	0.0061	0.0061	0.0061	0.0061	0.0060	0.0060	0.0060	0.0060
0.2	0.0244	0.0243	0.0242	0.0240	0.0239	0.0237	0.0235	0.0233	0.0231	0.0228
0.3	0.0547	0.0543	0.0538	0.0532	0.0524	0.0516	0.0507	0.0496	0.0483	0.0467
0.4	0.0967	0.0956	0.0941	0.0923	0.0900	0.0874	0.0841	0.0794	0.0738	0.0685
0.5	0.1503	0.1477	0.1442	0.1398	0.1342	0.1264	0.1153	0.1052	0.0965	0.0888
0.6	0.2151	0.2097	0.2027	0.1931	0.1786	0.1600	0.1437	0.1301	0.1187	0.1089
0.7	0.2907	0.2812	0.2679	0.2474	0.2178	0.1924	0.1716	0.1548	0.1406	0.1289
0.8	0.3767	0.3603	0.3362	0.2955	0.2558	0.2240	0.1995	0.1789	0.1624	0.1487
0.9	0.4720	0.4464	0.4023	0.3412	0.2929	0.2553	0.2258	0.2036	0.1846	0.1683
	Cap thickness $T_{cap} = 10$ μm									
0.0	0.0263	0.0263	0.0263	0.0262	0.0262	0.0263	0.0262	0.0263	0.0263	0.0262
0.1	0.0299	0.0305	0.0310	0.0312	0.0314	0.0315	0.0316	0.0317	0.0317	0.0318
0.2	0.0458	0.0474	0.0481	0.0484	0.0485	0.0483	0.0482	0.0480	0.0477	0.0474
0.3	0.0748	0.0763	0.0765	0.0759	0.0751	0.0743	0.0732	0.0722	0.0709	0.0693
0.4	0.1153	0.1157	0.1144	0.1123	0.1099	0.1071	0.1038	0.0993	0.0940	0.0889
0.5	0.1666	0.1646	0.1610	0.1562	0.1504	0.1427	0.1320	0.1224	0.1137	0.1066
0.6	0.2281	0.2231	0.2152	0.2052	0.1909	0.1728	0.1571	0.1438	0.1327	0.1237
0.7	0.2994	0.2896	0.2753	0.2553	0.2261	0.2017	0.1815	0.1648	0.1510	0.1399
0.8	0.3801	0.3638	0.3391	0.2985	0.2594	0.2291	0.2048	0.1852	0.1692	0.1561
0.9	0.4702	0.4434	0.3992	0.3395	0.2925	0.2566	0.2279	0.2056	0.1865	0.1717
	Cap thickness $T_{cap} = 20$ μm									
0.0	0.0370	0.0370	0.0370	0.0370	0.0370	0.0371	0.0370	0.0369	0.0370	0.0371
0.1	0.0398	0.0406	0.0412	0.0415	0.0417	0.0418	0.0419	0.0420	0.0420	0.0421
0.2	0.0539	0.0561	0.0571	0.0575	0.0575	0.0576	0.0574	0.0573	0.0571	0.0568
0.3	0.0809	0.0835	0.0839	0.0834	0.0826	0.0818	0.0810	0.0799	0.0787	0.0771
0.4	0.1197	0.1209	0.1196	0.1175	0.1153	0.1127	0.1093	0.1050	0.0998	0.0951
0.5	0.1688	0.1676	0.1634	0.1586	0.1529	0.1454	0.1354	0.1261	0.1180	0.1109
0.6	0.2277	0.2227	0.2146	0.2042	0.1905	0.1731	0.1584	0.1458	0.1348	0.1262
0.7	0.2955	0.2856	0.2710	0.2509	0.2230	0.1994	0.1802	0.1646	0.1512	0.1403
0.8	0.3718	0.3550	0.3309	0.2910	0.2536	0.2247	0.2015	0.1823	0.1677	0.1545
0.9	0.4571	0.4306	0.3867	0.3299	0.2849	0.2491	0.2224	0.2005	0.1829	0.1684
	Cap thickness $T_{cap} = 30$ μm									
0.0	0.0388	0.0386	0.0388	0.0388	0.0388	0.0388	0.0386	0.0388	0.0388	0.0388
0.1	0.0409	0.0418	0.0424	0.0427	0.0429	0.0433	0.0434	0.0435	0.0435	0.0437
0.2	0.0536	0.0561	0.0575	0.0578	0.0582	0.0582	0.0580	0.0578	0.0577	0.0574
0.3	0.0789	0.0822	0.0830	0.0826	0.0819	0.0811	0.0802	0.0792	0.0780	0.0766
0.4	0.1156	0.1180	0.1168	0.1150	0.1125	0.1101	0.1070	0.1030	0.0980	0.0935
0.5	0.1626	0.1620	0.1582	0.1537	0.1483	0.1409	0.1314	0.1228	0.1149	0.1084
0.6	0.2188	0.2142	0.2064	0.1970	0.1836	0.1673	0.1526	0.1407	0.1307	0.1222
0.7	0.2830	0.2737	0.2600	0.2412	0.2145	0.1914	0.1731	0.1585	0.1462	0.1356
0.8	0.3564	0.3398	0.3160	0.2784	0.2436	0.2151	0.1929	0.1753	0.1607	0.1488
0.9	0.4369	0.4111	0.3697	0.3150	0.2717	0.2387	0.2126	0.1920	0.1756	0.1616
	Cap thickness $T_{cap} = 40$ μm									
0.0	0.0368	0.0368	0.0367	0.0369	0.0368	0.0370	0.0368	0.0368	0.0368	0.0367
0.1	0.0387	0.0394	0.0401	0.0406	0.0409	0.0409	0.0413	0.0413	0.0414	0.0415
0.2	0.0503	0.0529	0.0542	0.0550	0.0553	0.0552	0.0552	0.0549	0.0548	0.0546
0.3	0.0742	0.0776	0.0787	0.0784	0.0777	0.0770	0.0762	0.0754	0.0740	0.0728
0.4	0.1090	0.1118	0.1111	0.1091	0.1071	0.1047	0.1016	0.0977	0.0935	0.0889
0.5	0.1536	0.1541	0.1503	0.1460	0.1404	0.1339	0.1250	0.1164	0.1094	0.1033
0.6	0.2069	0.2032	0.1962	0.1872	0.1743	0.1590	0.1454	0.1341	0.1243	0.1163
0.7	0.2683	0.2599	0.2467	0.2288	0.2037	0.1819	0.1652	0.1506	0.1385	0.1291
0.8	0.3380	0.3227	0.3005	0.2646	0.2315	0.2047	0.1835	0.1666	0.1529	0.1408
0.9	0.4149	0.3911	0.3516	0.2994	0.2583	0.2267	0.2019	0.1829	0.1668	0.1535

Table A.8. Thermal-neutron detector efficiencies for a square silicon cell of width W_{cell} and infinite in depth. A ^{6}LiF film of thickness T_{cap} coats one end. A 300-μm deep hole in the center of the cell with diameter D is filled with ^{6}LiF. Neutrons are incident normally and uniformly on the end opposite the cap. The detector cutoff energy E_{cut} is 300 keV.

D/W_{cell}	Cell Width X_{cap} (μm)									
	20	30	40	50	60	70	80	90	100	110
	Cap thickness $T_{cap} = 0$ μm									
0.0	0.0000	0.0000	0.0000	0.0000	0.0000	0.0000	0.0000	0.0000	0.0000	0.0000
0.1	0.0061	0.0061	0.0061	0.0061	0.0061	0.0061	0.0061	0.0061	0.0061	0.0061
0.2	0.0245	0.0245	0.0244	0.0243	0.0242	0.0240	0.0239	0.0237	0.0235	0.0233
0.3	0.0550	0.0548	0.0544	0.0539	0.0533	0.0526	0.0518	0.0508	0.0495	0.0481
0.4	0.0975	0.0967	0.0955	0.0940	0.0920	0.0896	0.0864	0.0818	0.0764	0.0713
0.5	0.1518	0.1498	0.1468	0.1429	0.1377	0.1302	0.1194	0.1096	0.1010	0.0935
0.6	0.2176	0.2132	0.2070	0.1982	0.1842	0.1660	0.1501	0.1367	0.1255	0.1160
0.7	0.2945	0.2864	0.2744	0.2549	0.2259	0.2010	0.1806	0.1641	0.1503	0.1388
0.8	0.3823	0.3680	0.3456	0.3060	0.2672	0.2358	0.2117	0.1916	0.1755	0.1619
0.9	0.4798	0.4568	0.4147	0.3552	0.3077	0.2710	0.2421	0.2200	0.2013	0.1856
	Cap thickness $T_{cap} = 10$ μm									
0.0	0.0265	0.0266	0.0265	0.0265	0.0265	0.0265	0.0265	0.0265	0.0265	0.0265
0.1	0.0301	0.0308	0.0313	0.0316	0.0318	0.0320	0.0321	0.0322	0.0322	0.0323
0.2	0.0464	0.0482	0.0491	0.0495	0.0495	0.0496	0.0495	0.0492	0.0490	0.0488
0.3	0.0765	0.0784	0.0788	0.0784	0.0777	0.0770	0.0760	0.0751	0.0738	0.0723
0.4	0.1190	0.1196	0.1186	0.1167	0.1147	0.1120	0.1089	0.1045	0.0991	0.0940
0.5	0.1724	0.1711	0.1679	0.1636	0.1582	0.1506	0.1399	0.1302	0.1216	0.1143
0.6	0.2367	0.2327	0.2255	0.2161	0.2022	0.1841	0.1682	0.1548	0.1436	0.1343
0.7	0.3115	0.3031	0.2901	0.2705	0.2415	0.2166	0.1961	0.1795	0.1654	0.1541
0.8	0.3965	0.3820	0.3586	0.3183	0.2791	0.2481	0.2236	0.2041	0.1875	0.1743
0.9	0.4917	0.4671	0.4245	0.3643	0.3167	0.2804	0.2513	0.2289	0.2094	0.1942
	Cap thickness $T_{cap} = 20$ μm									
0.0	0.0381	0.0380	0.0381	0.0380	0.0381	0.0380	0.0380	0.0380	0.0380	0.0380
0.1	0.0408	0.0416	0.0424	0.0427	0.0432	0.0431	0.0433	0.0435	0.0435	0.0436
0.2	0.0558	0.0585	0.0597	0.0602	0.0602	0.0604	0.0603	0.0602	0.0600	0.0597
0.3	0.0850	0.0881	0.0888	0.0884	0.0878	0.0870	0.0862	0.0853	0.0842	0.0827
0.4	0.1273	0.1290	0.1280	0.1260	0.1241	0.1216	0.1183	0.1140	0.1086	0.1036
0.5	0.1806	0.1800	0.1764	0.1721	0.1664	0.1589	0.1484	0.1388	0.1301	0.1227
0.6	0.2447	0.2406	0.2332	0.2235	0.2094	0.1910	0.1755	0.1625	0.1512	0.1419
0.7	0.3186	0.3098	0.2963	0.2765	0.2473	0.2225	0.2022	0.1856	0.1716	0.1601
0.8	0.4024	0.3874	0.3640	0.3231	0.2838	0.2531	0.2283	0.2084	0.1928	0.1790
0.9	0.4963	0.4718	0.4279	0.3683	0.3208	0.2833	0.2552	0.2323	0.2136	0.1980
	Cap thickness $T_{cap} = 30$ μm									
0.0	0.0413	0.0413	0.0412	0.0414	0.0414	0.0414	0.0412	0.0413	0.0413	0.0414
0.1	0.0435	0.0445	0.0453	0.0458	0.0461	0.0464	0.0465	0.0467	0.0467	0.0468
0.2	0.0578	0.0609	0.0625	0.0630	0.0635	0.0634	0.0635	0.0632	0.0631	0.0628
0.3	0.0864	0.0904	0.0916	0.0914	0.0909	0.0901	0.0893	0.0883	0.0870	0.0859
0.4	0.1286	0.1313	0.1305	0.1286	0.1266	0.1241	0.1210	0.1167	0.1112	0.1064
0.5	0.1821	0.1822	0.1787	0.1743	0.1688	0.1613	0.1508	0.1412	0.1325	0.1253
0.6	0.2462	0.2425	0.2349	0.2258	0.2115	0.1935	0.1774	0.1643	0.1531	0.1436
0.7	0.3200	0.3116	0.2978	0.2785	0.2494	0.2239	0.2038	0.1875	0.1737	0.1621
0.8	0.4042	0.3888	0.3651	0.3239	0.2855	0.2544	0.2297	0.2104	0.1941	0.1807
0.9	0.4974	0.4728	0.4293	0.3694	0.3211	0.2847	0.2562	0.2331	0.2147	0.1997
	Cap thickness $T_{cap} = 40$ μm									
0.0	0.0415	0.0414	0.0414	0.0414	0.0414	0.0413	0.0413	0.0414	0.0414	0.0413
0.1	0.0432	0.0443	0.0452	0.0456	0.0461	0.0464	0.0464	0.0467	0.0467	0.0468
0.2	0.0570	0.0605	0.0622	0.0630	0.0633	0.0634	0.0634	0.0632	0.0632	0.0629
0.3	0.0856	0.0901	0.0913	0.0914	0.0906	0.0902	0.0893	0.0883	0.0872	0.0857
0.4	0.1271	0.1310	0.1305	0.1285	0.1267	0.1243	0.1210	0.1166	0.1116	0.1062
0.5	0.1814	0.1819	0.1784	0.1741	0.1685	0.1612	0.1508	0.1409	0.1327	0.1256
0.6	0.2457	0.2421	0.2350	0.2253	0.2114	0.1935	0.1776	0.1647	0.1536	0.1436
0.7	0.3196	0.3113	0.2978	0.2781	0.2489	0.2241	0.2040	0.1872	0.1735	0.1619
0.8	0.4037	0.3888	0.3648	0.3243	0.2858	0.2543	0.2300	0.2101	0.1943	0.1804
0.9	0.4976	0.4729	0.4292	0.3690	0.3216	0.2846	0.2554	0.2335	0.2148	0.1991